Intra-specific variability in plant hydraulic parameters inferred from model inversion of sap flux data

Yaojie Lu[1], Brandon Sloan[1,2], Sally E. Thompson[3], Alexandra G. Konings[4], Gil Bohrer[5], Ashley Matheny[6], Xue Feng[1,2]

[1]Department of Civil, Environmental, and Geo-Engineering, University of Minnesota, Minneapolis, MN 55455, USA

[2]Saint Anthony Falls Laboratory, University of Minnesota, Minneapolis, MN 55455, USA

[3]Department of Civil, Environmental and Mining Engineering, University of Western Australia, WA 6009, Australia

[4]Department of Earth System Science, Stanford University, CA, 94305, USA

[5]Department of Civil, Environmental, and Geodetic Engineering, The Ohio State University, OH 43210, USA

[6]Department of Geological Sciences, Jackson School of Geosciences, University of Texas at Austin, Austin, TX, USA

Corresponding authors:

Yaojie Lu: https://orcid.org/0000-0002-5215-6109; tanisraistlin@gmail.com;

Xue Feng: https://orcid.org/0000-0003-1381-3118; feng@umn.edu

Key points

- Plant hydraulic parameters are inferred with low uncertainty from sap flow data
- Inferred parameter values capture whole-plant response and water use strategies instead of leaf or branch-level responses
- The model inversion method complements field measurement of plant hydraulic traits

Abstract

Understanding plant hydraulic regulation is critical for predicting plant and ecosystem responses to projected increases in drought stress. Plant hydraulic regulation is controlled by observable, diverse plant hydraulic traits that can vary as much across individuals of the same species as they do across different species. Direct measurements of plant hydraulic traits from a range of ecosystems remain limited in comparison to other, more readily measured traits (e.g., specific leaf area). Furthermore, plant hydraulic trait measurements, often made at leaf or branch levels, are not easily scaled to whole-plant values that are typically used to predict plant and ecosystem fluxes. In this study, multiple whole-plant hydraulic parameters are inferred from observations of plant water use (i.e., sap flow), soil properties, and meteorological data. We use a Markov Chain Monte Carlo model inversion approach to obtain the best estimates and uncertainty of plant hydraulic parameters that capture whole-plant effective embolism resistance and stomatal sensitivity to decreasing plant water potential. We then use the inferred values in the model to estimate whole-tree water use and isohydricity. This approach reliably infers whole-plant parameter values with enough specificity to resolve inter- and intra-specific differences, and thus supplements time- and labor-intensive direct measurements of traits.

Key words: plant hydraulics, xylem vulnerability, model inversion, MCMC, sap flow

1 Introduction

The increasing frequency and severity of drought in many parts of the world (Field et al. 2012) contributes to water stress (Dai, 2011; Feng et al., 2019; Williams et al., 2013) and mortality in plant communities (Allen et al., 2010; De Kauwe et al., 2020; McLaughlin et al., 2020; Novick et al., 2016; Young et al., 2017), with subsequent changes in ecosystem water, carbon, and energy cycling (Bonan, 2008). Plant response and vulnerability to drought, as well as recovery after drought, are controlled by a combination of root, xylem, and leaf hydraulic traits and stomatal responses. For example, under drought conditions, stomatal closure closely coordinates with xylem resistance to embolism (measured by the water potentials at 12% (P12) and 50% (P50) loss of conductance in xylem) across different taxonomic (gymnosperm and angiosperm) and functional (evergreen and deciduous) groups to regulate plant water use, plant water potential, and the extent of xylem embolism (Bartlett et al., 2016; Martin-StPaul et al., 2017). This coordination of multiple plant hydraulic traits, including stomatal control and xylem embolism resistance, also influence the timing of hydraulic failure in plants (Blackman et al., 2019). Finally, by regulating whole-tree carbon allocation, plant hydraulic traits, including P50 and maximum xylem hydraulic conductance, can explain leaf area dynamics, delayed mortality, and xylem damage recovery post drought (Trugman et al., 2019, 2018).

Plant hydraulic traits are also critical for prediction, particularly as; parameters in physically-based Plant Hydraulic Models (PHMs). PHMs represent water transport through the soil-plant-atmosphere continuum via flux-gradient relationships (based on Hagen-Poiseuille flow or porous media flow). Hydraulic parameters are needed to describe the functional form of their conductance vulnerability curves (Mencuccini et al., 2019) and stomatal responses (Mirfenderesgi et al., 2019). The recent implementations of PHMs into terrestrial biosphere

63 models have shown promising corrections of previous prediction biases in gross primary
64 productivity and evapotranspiration (Bonan et al., 2014; Eller et al., 2020; Kennedy et al., 2019;
65 Li et al., 2021; Powell et al., 2013; Sabot et al., 2020; Xu et al., 2016) as well as soil water
66 balance (Kennedy et al., 2019), especially under drought conditions. However, the use of PHMs
67 in models is still hindered by the need to acquire plant hydraulic traits for parameterization
68 (Feng, 2020; Paschalis et al., 2020; Sloan et al., 2021).

69 Plant hydraulic traits exhibit large intraspecific (Martínez-Vilalta et al., 2009; Pritzkow et al.,
70 2020; Rosas et al., 2019) and interspecific variability (Choat et al., 2012; Maherali et al., 2006)
71 that must be accounted for when considering ecosystem-level response to drought. For example,
72 trait interspecific variability better explains interannual variability in the ecosystem fluxes of
73 carbon, water, and energy at global scales than do community-weighted trait values (Anderegg et
74 al., 2018). Although no comprehensive assessment of intraspecific variability exists, one meta-
75 analysis has shown that intraspecific variability of P50 can account for a significant portion
76 (33%) of interspecific variability within a genus (Anderegg, 2015). Therefore, a detailed
77 characterization of both inter- and intraspecific hydraulic trait variability is necessary for
78 predicting ecosystem response to drought.

79 Despite the obvious need, comprehensive plant hydraulic trait measurements are far less
80 available than many other plant traits, e.g., specific leaf area (Belluau and Shipley, 2018). This
81 limitation may be attributed to the time-consuming and expensive nature of hydraulic trait
82 measurements. For example, the traditional bench dehydration technique to measure P50 at leaf
83 or branch scales usually takes hours to days for samples to dehydrate and requires multiple
84 measurements of water potentials (Tyree and Sperry, 1988). Additionally, hydraulic trait
85 measurements commonly made at leaf or branch scales are difficult to scale up to the

representative whole-plant parameter values required for modeling plant hydraulic regulation. To address these data needs, in this study, we aim to facilitate the estimation of plant hydraulic traits by using a model inversion approach to infer whole-plant parameter values, and their associated variability, indirectly from existing sap flow measurements. Model inversion allows the use of existing data (e.g., sap flow) to constrain the model parameters that represent effective whole-plant hydraulic traits, yielding parameter estimates enabling the model to best approximate reality (Luo et al., 2011). We focus on sap flow because it provides species-specific observation of transpiration, rather than the plot level estimate provided from eddy covariance flux towers, which mix the contribution of all species in a large observation footprint.

Among common model inversion techniques (e.g., frequentist methods or Kalman filter, (Mo et al., 2008)), we select Markov Chain Monte Carlo (MCMC) for parameter estimation, primarily because it quantifies the epistemic uncertainty associated with each model parameter in addition to its best estimates (Wu et al., 2014). It has also been successfully used for inversion of plant hydraulic models in eddy covariance (Liu et al., 2020) and remote sensing (Liu et al., 2021) settings. In our case, we use MCMC to estimate the whole-plant effective values of plant hydraulic traits as parameters in a physiologically informed sap flow model using local soil water potential and atmospheric conditions as inputs to the model. The model includes the following hydraulic trait parameters: P50, stomatal sensitivity to decreasing water potential, a scaling parameter from the model of Medlyn et al., (2011), which is inversely proportional to plant marginal water-use efficiency, and two more parameters aggregating maximum plant hydraulic conductance, leaf area, and sapwood area per ground area (see Tables 2 & 4) as these traits cannot be inferred independently (see Section 2.2 Sap flow model).

The uncertainty estimates provided by MCMC also allow for further investigation of the factors contributing to the parameter uncertainties. Parameter uncertainties are important because they determine the range of potential model outcomes. Of the multiple sources of uncertainty that can affect parameter estimates (Raupach et al., 2005), we will investigate the relative contributions of (1) low model sensitivity to parameters; (2) measurement error; and (3) lack of prior knowledge about the unknown parameters. Note that we assume a single model structure with enough flexibility to simulate observed plant hydraulic behavior (Xiao et al., 2014) and do not attempt to quantify the role of uncertainty in the model structure.

This paper aims to address the following questions: 1) Can MCMC be used to reliably infer inter- and intra- specific variability in plant hydraulic parameters using measurements of sap flow, meteorological, and soil moisture data? 2) To what extent do model sensitivity, measurement error, and lack of prior knowledge contribute to the uncertainty associated with parameter estimates? Additionally, compared to other environmental variables that are commonly measured (e.g., air temperature, solar irradiance, or vapor pressure deficit), far fewer measurements of soil water potential are taken in the field. Thus, we also ask 3) What is the consequence of missing or biased measurements of soil water potential during parameter inference? By addressing these questions, we demonstrate that MCMC model inversion can be applied to the increasingly available environmental and sap flow data from sap flow monitoring networks (e.g., SAPFLUXNET, Poyatos et al., 2019) to reliably infer difficult-to-measure hydraulic parameters and advance our understanding and prediction of ecosystem response to climate change.

2 Materials and Methods

2.1 Site and data description

The study site consists of temperate mixed forest located within the footprint of the US-UMB Ameriflux eddy covariance tower at the University of Michigan Biological Station (UMBS) in northern Michigan, U.S.A. The long-term mean annual precipitation for the region is 766 mm with a mean annual temperature of 5.5 °C (Matheny et al., 2017). Local soils are composed of 92.2% sand, 6.5% silt, and 0.6% clay (Nave et al., 2011). The UMBS forest is a relatively evenly aged stand (mean tree age ~95 years) transitioning from an aspen (*Populus grandientata*) and birch (*Betula papyrifera*) dominated stand to one dominated by red maple (*Acer rubrum*), white pine (*Pinus strobus*), red oak (*Quercus rubra*), American beech *(Fagus grandifolia*), and sugar maple (*Acer saccharum*). The primary research area consists of the 180 ha footprint of the US-UMB flux tower. In this area, stand density is roughly 750 trees per hectare, mean canopy height is ~25m, and mean growing-season peak leaf area index is, on average, 3.9 m^2m^{-2}. Additional relevant hydrophysiological and stand contribution data are presented in Table 1.

Table 1. Additional hydrophysiological and stand contribution data, including average diameter at breast height (DBH) of instrumented trees (cm), average height of instrumented trees (m), fraction of total stand area (%), average leaf to sapwood area of instrumented trees (m^2 m^{-2}), xylem architecture, isohydricity, wood density (g cm^{-3}).

	Average DBH cm (± std)	**Average Height m (± std)**	**Fraction of total stand area**	**Average leaf to sapwood area (m^2m^{-2})**	**Xylem architecture**	**Isohydricity**	**Wood Density (g cm^{-3})**
Red maple	15.16 (5.2)	19.69 (7.6)	19.48%	2161.8	Diffuse porous	Isohydric	0.546
Paper birch	17.14 (5.3)	24.08 (7.9)	7.79%	1365.8	Diffuse porous	Unknown	0.600
Bigtooth aspen	23.48 (4.5)	28.98 (6.4)	52.27%	897.1	Semi-ring porous	Relatively anisohydric	0.412
White pine	11.5 (5.4)	13.01 (5.0)	8.44%	4165.4	Tracheid	Unknown	0.373

Meteorological measurements, including air temperature, T (°C), relative humidity, RH (unitless), and photosynthetic photon flux density, I (μmol m^{-2} s^{-1}), were collected at the eddy-covariance tower at one-minute intervals. Relative volumetric soil water contents, s_d (%), were measured near the tower at the depths d of 15, 30, and 60 cm at ten-minute intervals. All meteorological and soil observations were averaged to half-hourly resolution. We obtained the processed half-hourly observation from Ameriflux, site US-UMB (Gough et al., 1999). Measurement setup and error correction are detailed elsewhere for meteorological conditions (Gough et al., 2013) and volumetric soil water content (He et al., 2013).

Leaf-to-air vapor mole fraction difference (the leaf-to-air vapor pressure difference divided by atmospheric pressure), D (unitless), was calculated from air temperature and humidity data following Monteith and Unsworth (2013):

$$D = \frac{(1 - RH) D_a \, exp\left(\frac{D_b T}{T + D_c}\right)}{D_d} \quad (1)$$

where D_a, D_b, and D_c are model parameters with values of 0.61, 17.27, and 237.3, respectively. D_d is the atmospheric pressure, assumed to have a standard value of 101.3 kPa. Soil water potential at each depth, Ψ_{sd} (MPa), was calculated from s_d using the van Genuchten model (Hou and Rubin, 2005; van Genuchten, 1980)

$$\Psi_{sd} = \frac{s_b}{s_a}\left(\left(\frac{s_s - s_r}{s_d - s_r}\right)^{\frac{\eta}{\eta - 1}} - 1\right)^{\frac{1}{\eta}} \quad (2)$$

where s_a, s_r, s_s, and η are fitted parameters from a previous analysis at our site (see details in He et al., 2014) with values of -5.2, 0.04, 0.37, and 1.68, respectively. The term s_b (=0.0098)

converts water potential from m to MPa. The s_d measurements were used to calculate Ψ_{sd} and, in turn, the depth-averaged soil water potential Ψ_s.

Sap flow per sapwood area, v_n (g H_2O m^{-2} xylem s^{-1}), was monitored for individual trees at one-minute intervals and averaged to half-hourly intervals (Matheny et al., 2017). Sap-flux data for the US-UMB site was obtained from SAPFLUXNET (Poyatos et al., 2020, 2016). We assumed all trees experienced the same environmental conditions measured from one location (i.e., the measurements of T, I, D, and s_d at all the depths). Further site details on sap-flow data collection can be found in Matheny et al. (2014). Measurements were available from 2010 to 2016, and we focused on the year 2015 as it had the greatest amount of data available. Of the sap flux data available for the site, we excluded measurements from trees with more than 20% missing values. Furthermore, we removed two individuals showing irregular sap flow dynamics: one maintained 90% of maximum sap flow regardless of Ψ_s, and another's sap flow dropped to zero when $\Psi_s < -0.5$ MPa, while all other individuals had non-zero sap flow over the whole period. In total, this study used observations from 23 individual trees of four canopy-dominant species: 8 red maple, 5 paper birch, 5 bigtooth aspen, and 5 white pine trees.

Finally, we converted the half-hourly data to daily for all of the variables. We used only measurements under high solar irradiance (i.e., I > 10 μmol m^{-2} s^{-1}), assuming that these measurements corresponded to periods of active transpiration. With this subset of high irradiance, we calculated the daily mean values for T, I, and v_n, the daily minimum value for Ψ_s, and the daily maximum value for D. For conciseness, we used the same symbols for all the variables before and after the conversion to daily values. In summary, our dataset consisted of the daily measurements of T, I, D, and Ψ_s, at the site level and v_n at the individual level.

2.2 Sap flow model

We aimed to infer whole-plant hydraulic parameters using MCMC inversion of a whole-plant, daily-averaged sap flow model in combination with the sap flow data of individual trees and local soil water potential and atmospheric data. Our model targets the bulk water transport within plants and thus excludes the complexities of belowground water movement (e.g., resistance between soils and roots) and assumes the soil water potential is representative of conditions near plants' fine roots. In addition, this model does not account for plant water-storage effects and assumes that its effect on variations in plant hydraulic conductance is smoothed out over time.

The sap flow model is derived from equations of plant hydraulics and stomatal regulation. First, we assume that daily, whole-plant transpiration, E (m^3 m^{-2} ground s^{-1}), is determined by the balance between stomatal-mediated transpiration from atmospheric demand and the supply of water transported from soil to leaf driven by water potential differences (McDowell and Allen, 2015):

$$E = a \cdot l \cdot L \cdot g_s \cdot D = 10^{-3} \cdot l \cdot k_x(\Psi_x) \cdot (\Psi_s - \Psi_x) \quad (3)$$

where a (=1.6) is the ratio of water vapor and CO_2 diffusivities, l (m^3 mol^{-1}) converts H_2O from mol (gas) to m^3 (liquid), L (m^2 leaf m^{-2} ground) is leaf area index, g_s (mol m^{-2} leaf s^{-1}) is stomatal (and aerodynamic) conductance, Ψ_x (MPa) is plant water potential, and k_x (Ψ_x) (mmol m^{-2} ground s^{-1} MPa^{-1}) is the whole-plant effective xylem hydraulic conductance (Eq. 4). Due to lack of data, we assume leaf area index remains constant over the whole observation period and infer its value. Because we focus our analysis on the peak of the growing season between May 30, 2015, and September 16, 2015, we expect all species were equally affected by this assumption of constant leaf area index. All the fitting parameters are listed in Table 2 and model parameters with prescribed values in Table 3.

The function k_x (Ψ_x) represents reducing whole-plant hydraulic conductance with decreasing Ψ_x due to xylem embolism. Following Martin-StPaul et al., (2017), xylem conductance is modeled by

$$k_x(\Psi_x) = k_{xmax} \cdot \left(1 - \frac{1}{1 + e^{\frac{k_a + k_b e^{P_{50}}}{k_c} \cdot (\Psi_x - P_{50})}}\right) \quad (4)$$

where k_{xmax} (mmol m^{-2} ground s^{-1} MPa^{-1}) is the maximum, whole-plant xylem hydraulic conductance, P50 (MPa) is the Ψ_x at 50% loss of k_x, and k_a, k_b, and k_c are all fitting parameters from Martin-StPaul et al., (2017) with values of 16, 1092, and 25, respectively.

In order to represent stomatal regulation on transpiration we use the following empirical model of stomatal conductance:

$$g_s = \left(1 + \frac{g_1}{\sqrt{D}}\right) \cdot \frac{A(g_s, T, I)}{c_a} \cdot e^{(-c \cdot f_{PLC}(\Psi_x))} \approx \frac{g_1}{\sqrt{D}} \cdot \frac{A(g_s, T, I)}{c_a} \cdot e^{(-c \cdot f_{PLC}(\Psi_x))} \quad (5)$$

where the percentage of loss in xylem conductivity, f_{PLC} (unitless), is defined as

$$f_{PLC}(\Psi_x) = 1 - \frac{k_x(\Psi_x)}{k_{xmax}}; \quad (6)$$

g_1 (unitless) is inversely related to plant marginal water use-efficiency (Medlyn et al., 2011), the function A (μmol m^{-2} leaf s^{-1}) is the carbon assimilation rate as determined by the Farquhar-von Caemmerer-Berry photosynthesis model (Farquhar et al., 1980), c_a (ppm) is the ambient CO_2 concentration, and c (unitless) represents stomatal sensitivity to decreasing water potential (i.e., stomatal drought sensitivity). We use species-specific values (i.e., the mean values in the TRY database, Kattge et al., (2020)) of photosynthetic carboxylation capacity (V_{cmax}) and photosynthetic electron transport capacity per leaf area (J_{max}) at 25°C. The parameters V_{cmax} (micro mol m^{-2} s^{-1}) and J_{max} (micro mol m^{-2} s^{-1}) are set to be: 31 and 48 for red maple; 56 and

144 for paper birch, 61 and 122 for bigtooth aspen, and 63 and 142 for white pine. The first two terms in Eq. 5 follow Medlyn et al., (2011) who has also shown that the term $g_1/\sqrt{D}$ tends to dominate the term $\left(1 + g_1/\sqrt{D}\right)$. The last exponential term captures the generally observed Weibull stomatal closure to plant water potential (Klein, 2014). The choice to independently downregulate stomatal conductance with plant water potential follows Jarvis (1976) as well as similar formulations derived from optimal stomatal response under water stress (Manzoni et al., 2011; Zhou et al., 2013; Wolf et al., 2016). Although questions exist around *a priori* defining a $g_s - \Psi_x$ relationship (Anderegg and Venturas, 2020), this formulation remains common in PHM implementation for terrestrial biosphere models (De Kauwe et al. 2015; Xu et al., 2016; Christofferson et al., 2016; Kennedy et al., 2019).

Lastly, under the assumptions that sap flow measurements are taken on the main stem and there is no storage in the tree, we model E to be proportional to sap flow, v_n (g H_2O m^{-2} xylem s^{-1}) as follows:

$$\frac{v_n \cdot \alpha}{\rho} = E \tag{7}$$

where α (m^2 sapwood m^{-2} ground) is the sapwood area per ground area; ρ (=997,000 g m^{-3}) is the water density.

In the sap flow model consisting of Eqs. 3-7, we defined six unknown parameters: L, k_{xmax}, P50, g_1, c, and α (Table 2). By simply rearranging the above equations, we can show that k_{xmax}, L and α cannot be inferred independently. Instead, they can only be inferred in an aggregated form - here as k_{xmax}/L and α/L. To demonstrate this, we combine Eqs. 3-5 and solve for g_s to obtain

$$g_s = \frac{k_{xmax}}{L} \cdot \frac{10^{-3}\left(1 - f_{PLC}(\Psi_x)\right) \cdot (\Psi_s - \Psi_x)}{a \cdot D}. \quad (8)$$

245 Then, by expanding Eq. 7 using Eqs. 3-6, we obtain

$$v_n = 10^{-3} \cdot \rho \cdot l \cdot \frac{\frac{k_{xmax}}{L}}{\frac{\alpha}{L}} \cdot \left(1 - f_{PLC}(\Psi_x)\right) \cdot (\Psi_s - \Psi_x). \quad (9)$$

246 Now Eqs. 6, 8 & 9 define the complete sap flow model by Eqs. 3-7. We can solve them for the
247 three unknown state variables (i.e., g_s, Ψ_x, and v_n). Notice that L, k_{xmax}, and α now only appear in
248 an aggregated form as k_{xmax}/L and α/L. Consequently, we can infer five unknown parameters
249 independently (i.e., Ψ_{x50}, g_1, c, k_{xmax}/L and α/L).

250 **Table 2.** Description of symbols, along with definitions, units of measurement of the unknown
251 model parameters

Symbol	Definition	Unit
c	Stomatal sensitivity to decreasing xylem water potential	–
g_1	Fitting parameter from Medlyn et al., (2011)	–
k_{xmax}	Maximum whole-plant xylem conductance	mmol m^{-2} ground s^{-1} MPa^{-1}
L	Leaf area index	m^2 leaf m^{-2} ground
α	Sapwood area per ground area	m^2 sapwood m^{-2} ground
P50	Xylem water potential at 50% loss of conductivity	MPa

252

253 **Table 3.** Description of symbols, along with definitions, units of measurement, and default
254 parameter values. For a model variable, its definition equation is given in the 'Value' column.
255 For an input variable, its value is given as '– '.

Symbol	Definition	Unit	Value
A	Ratio of the diffusivities of water vapor and air	–	1.6
c_a	Ambient CO_2 concentration	ppm	400
g_s	Stomatal conductance to CO_2	mol m^{-2} leaf s^{-1}	Eqs. 3 & 6
k_x	Xylem hydraulic conductance	mmol m^{-2} ground s^{-1} MPa^{-1}	Eq. 4
L	Converting H_2O from mol (gas) to m^3 (liquid)	m^3 mol^{-1}	1.8×10^{-5}
v_n	Daily-averaged sap flow	g H_2O m^{-2} xylem s^{-1}	–
A	Photosynthesis rate	μmol m^{-2} leaf s^{-1}	
D	Leaf-to-air vapor mole fraction difference	–	–
E	Transpiration rate	m^3 m^{-2} ground s^{-1}	Eq. 3
I	Solar irradiance	μmol m^{-2} s^{-1}	–
f_{PLC}	Percentage loss of hydraulic conductivity	–	Eq. 6
T	Temperature	^0C	–
ρ	Water density	g m^{-3}	997000
Ψ_s	Soil water potential	MPa	–
Ψ_x	Xylem water potential	MPa	Eqs. 3 & 6

2.3 MCMC implementation

We estimated the fitting parameters for each individual tree using MCMC. The MCMC updates the prior distribution of each fitting parameter based on the available data, including T, I, D, Ψ_s, and v_n. The assumed prior distribution of each unknown parameter is given in Table 4. The prior distributions were selected to 1) reflect reasonable and physically realistic ranges of each parameter (Kattge et al., 2020 for P50; Li et al., 2018 for c; Lin et al., 2015 for g_1; Matheny et al., 2014 for α/L; Mirfenderesgi et al., 2019 for k_{xmax}/L) and 2) result in peaked P50 posterior distribution within the support of its prior distribution. The prior distributions given in Table 4 were applied to all individuals with exception of the three paper birch individuals. For these individuals, we had to use a modified prior distribution of c with a smaller support (Uniform: [5, 10]) for the posterior distribution of P50 to be peaked within the support of its prior distribution. MCMC was implemented in Python using the PyMC package (Patil et al., 2010).

Table 4. Prior distribution of the unknown parameters. The prior distributions were selected to reflect reasonable and physically realistic ranges of each parameter.

Symbol	Prior distribution
c	Uniform: [5, 30]
g_1	Uniform: [0.01, 1]
k_{xmax}/L	Log uniform: [0, 3]
α/L	Log uniform: [-5, 0]
P50	Uniform: [-5, -0.1]

2.4 Synthetic experiments

We use three synthetic experiments to examine the impacts of 1) measurement error and 2) prior knowledge on the accuracy of the estimated parameter – two of the three sources of estimation uncertainty investigated in this study. Two synthetic experiments will address two types of measurement errors: 1) the noise in sap flow data and 2) the bias in soil water potential. The reason we choose to focus on the bias rather than the noise in soil water potential as a measurement error is that it is more likely that the sitewide soil water potential used in this study is consistently higher or lower than the actual soil water potential for every individual tree. The third synthetic experiment will examine the effect of limited prior knowledge on the posterior distribution.

In the first synthetic experiment, we simulate noisy sap flow measurements by generating synthetic sap flow data over a series of noise levels . We generate the baseline synthetic sap flow data with zero noise by running the sap flow model forwards with prescribed parameter values (c = 13, g_1 = 20, k_{xmax}/L = 1000, α/L = 0.01, P50 = -2.5) and the measured environmental inputs from the UMBS dataset. We then generate five sets of noisy sap flow data by adding Gaussian noise with zero mean to the synthetic baseline sap flow data, each with a different level of correlation to the synthetic baseline sap flow data itself. The correlation coefficients between the baseline synthetic sap flow data and the five sets of noisy sap flow data are 0.95, 0.9, 0.85, 0.8, and 0.75. We then infer the hydraulic parameters using the MCMC process, after replacing observed UMBS sap flux with the six synthetic datasets (which consist of noise-free baseline or noisy synthetic sap flow data and the environmental input data of T, I, D, and Ψ_s from the UMBS dataset) and compare the estimated hydraulic parameters with the true (i.e. prescribed) parameter values.

In the second experiment, we create the baseline synthetic soil water potential data by first lowering the soil water potential data from the UMBS dataset by an artificial bias of 1 MPa. This reduction avoids the risk of generating positive soil water potential values in the synthetic soil water potential data that are to be created subsequently. We generate the synthetic sap flow data by running the sap flow model forwards with this baseline synthetic soil water potential data, the prescribed parameter values (the same as in the first experiment, $c = 13$, $g_1 = 20$, $k_{xmax}/L = 1000$, $\alpha/L = 0.01$, P50 = -2.5), and the original data for the other environmental inputs (i.e., T, I, and D) from the UMBS dataset. Then, to simulate the biased soil water potential measurement, we generate two biased sets of synthetic soil water potential data by setting their values to be consistently lower and higher than the baseline synthetic soil water potential data by 1 MPa over the whole period, respectively, while using the same data from the baseline dataset for all the other inputs, including T, I, D, and modeled sap flow. Finally, to evaluate the effect of bias in soil water potential measurement on parameter estimation, we infer the hydraulic parameters estimated from MCMC using these three synthetic datasets and compare them to the synthetic truth.

In the third experiment, to examine the effect of prior knowledge on parameter estimation, we also use the baseline synthetic dataset from the first synthetic experiment. Two prior distributions, the uniform, and a truncated normal distribution, are proposed to represent low and high amounts of prior information concerning parameters, respectively. By comparing the results of posterior distributions, we can evaluate the effect of prior information on parameter inference.

2.5 Sensitivity analysis

316 To explore the effect of parameter sensitivity – our final source of uncertainty – on parameter
317 inference, we carry out a Sobol global sensitivity analysis (Sobol, 2001) to identify the
318 importance of each parameter in determining the model output (i.e., sap flow). We expect a
319 parameter with a higher sensitivity to have a lower variance in its posterior distribution. The
320 first-order indices from a Sobol sensitivity analysis measure the contribution to the output
321 variance of the main effect of each parameter (i.e., the effect of varying each parameter alone)
322 while the total-order indices measure the output variance of each parameter, including all
323 variance caused by its interaction with any other parameters. For each parameter, we define its
324 parameter range for the sensitivity analysis based on the supports of its posterior distributions of
325 all the tree individuals from the UMBS dataset, which we consider as the realistic parameter
326 range.

327 Because the soil water potential data is not as widely available as the other environmental
328 conditions (e.g., T, I, and D), we examine the effects of soil water potential data availability on
329 the resulting model sensitivities by running the sensitivity analysis with Ψ_s as either a known
330 input or as an unknown constant. Based on the sensitivity of soil water potential and its influence
331 in the sensitivities of other unknown parameters, we evaluate the importance of the availability
332 of soil water potential data. We define the range for soil water potential (when treating it as an
333 unknown parameter) based on the maximum and minimum values in the UMBS dataset. In the
334 first scenario, Ψ_s data is considered to be available – we use the complete set of environmental
335 inputs, including T, I, D, and Ψ_s, from the UMBS dataset as the known environmental inputs for
336 the sensitivity analysis. In the second scenario, we run the sensitivity analysis with the soil water
337 potential as an unknown constant. We repeat this analysis independently on every single day
338 with varying environmental conditions over the whole observation period in both scenarios.

2.6 Prediction of sapflow and whole-tree water use behaviors

To verify that the inferred hydraulic traits can indeed be used to predict whole-plant water use behaviors, we compared our predicted sap flow against existing measurements. Furthermore, we contextualized the plant water-use strategy under water stress using the isohydricity framework proposed by Martinez-Vilalta et al. (2014). We use the median predicted plant water potential (ψ_x) and the input soil water potential (ψ_s) to fit a simple linear relationship, $\psi_x = \sigma\psi_s + \Lambda$, where the intercept ($\Lambda$) represents the plant water potential under well-watered conditions ($\psi_s \approx 0$) and the slope (σ) indicates stomatal response to soil water stress, i.e., isohydricity. An isohydric plant will have $\sigma \approx 0$ as it will close stomata to maintain a near-constant ψ_x value regardless of ψ_s, representing a more risk-averse strategy to hydraulic damage. Alternately, as σ increases, the plant moves towards anisohydric behavior, where it allows ψ_x to decline (by regulating stomata less) with ψ_s in order to prolong transpiration at the risk of hydraulic damage. Although there are confounding factors to the isohydricity concept (Novick et al., 2019; Feng et al., 2019), σ nevertheless provides useful insight into the inter- and intraspecific variability of plant water use strategies (Kannenberg et al., 2021). We fit the isohydricity index, σ, to each site and performed a species-level comparison using a single factor ANOVA and pairwise t-tests using Tukey's HSD test to determine if σ values for each species differed and by how much. Tukey's HSD allows pairwise t-tests while accounting for p-value inflation while performing multiple hypothesis tests (Efron and Hastie, 2016). We performed ordinary least squares fitting and hypothesis testing using the statsmodel package in Python (Seabold and Pektold, 2010).

3 Results

We first present the results of MCMC inversion of our sap flow model, including the posterior distributions, the ensemble prediction of sap flow, as well as the estimated isohydricity based on predictions of plant water potential. Then, we analyze the uncertainties associated with parameter estimation, due to 1) low parameter sensitivity, 2) measurement error, including the noise in sap flow data and the bias in soil water potential, and 3) the lack of prior information on the fitting parameters. The sensitivities of model parameters are represented by Sobol first-order and total-order sensitivity indices. We demonstrate the effects of measurement error and prior information based on three synthetic experiments, then, based on these results, make recommendations to potentially reduce estimation errors.

3.1 MCMC inference of plant hydraulic parameters

The whole-plant effective value of xylem water potential at 50% loss of hydraulic conductivity, P50, is an important trait that characterizes plant drought tolerance (Brodribb and Cochard, 2009). In Fig. 1a, we show the posterior distributions of P50 for each individual. All the P50 estimates have low uncertainty, with a maximum coefficient of variation below 0.08 and standard deviation below 0.2 MPa. These posterior distributions show an order of magnitude reduction in uncertainty compared to the prior distribution of P50, which is uniformly distributed between -5 MPa and -0.1 MPa. This low uncertainty allows us to easily detect both the inter- and intraspecific difference in P50. Generally, red maple and white pine have similar inferred P50 values at around -1.5 MPa (Fig. 1a). Paper birch and bigtooth aspen have slightly more negative P50 at around -2.0 MPa. Fig. 1b shows measured P50 values compiled from the TRY dataset and other literature sources (Deacon et al., 2019; Kattge et al., 2020, Fig. 1b) for each of these species. For red maple, the inferred P50 values are at the higher bound of the P50 data from the TRY database. This difference relative to previous measurements may be due to intra-specific

variability, or may be related to the fact that, unlike the field measurements of P50, which are commonly made at leaf or branch scales, our inferred P50 values represent the effective whole-plant value of this trait. Specifically, based on a modeling analysis (see Supporting Information, Fig. S1), we show that the effective whole-plant P50 is more likely to be lower than the segment P50 in the roots, and higher in the segments that are further away from the soil (i.e., closer to leaves). The P50 data for the other species are scarce (three data points for paper birch (Kattge et al., 2020); one for bigtooth aspen (Deacon et al., 2019), and none for white pine), although our estimates of P50 for paper birch and bigtooth aspen are still consistent with measurements.

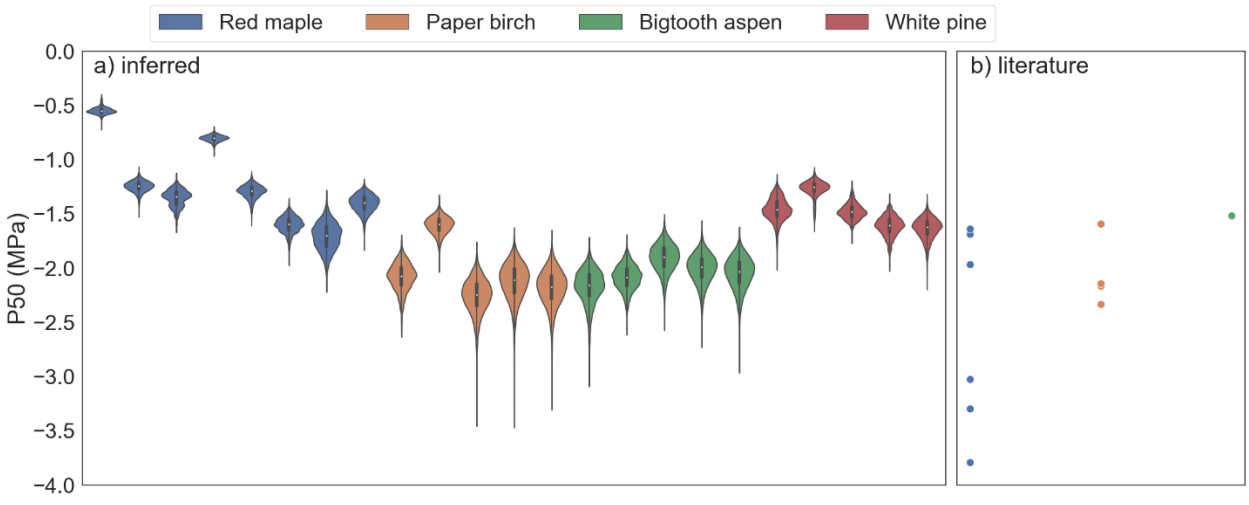

Figure 1. a) Posterior distributions of P50. Each bar represents an individual tree. Color indicates species: blue for red maple, yellow for paper birch, green for bigtooth aspen, and red for white pine. b) Measurements from the literature (data for red maple and paper birch are from the TRY database (Kattge et al., 2020); data for bigtooth aspen are from Deacon et al., (2019); no data have been found for white pine).

We quantified the intraspecific variation in P50 using the coefficient of variation of the mean of the posterior distributions of all the individuals from the same species. Red maple shows the

399 greatest intra-specific variability in Fig. 1a and has a higher standard deviation in the mean (0.36
400 MPa) across individuals than the rest (0.23 for paper birch; 0.09 for bigtooth aspen; 0.13 for
401 white pine). Compared with the species-level mean P50, none of the species shows a coefficient
402 of variation higher than 0.3 (0.29 for red maple; 0.11 for paper birch; 0.04 for bigtooth aspen;
403 0.09 for white pine), indicating a low intraspecific variation in P50.

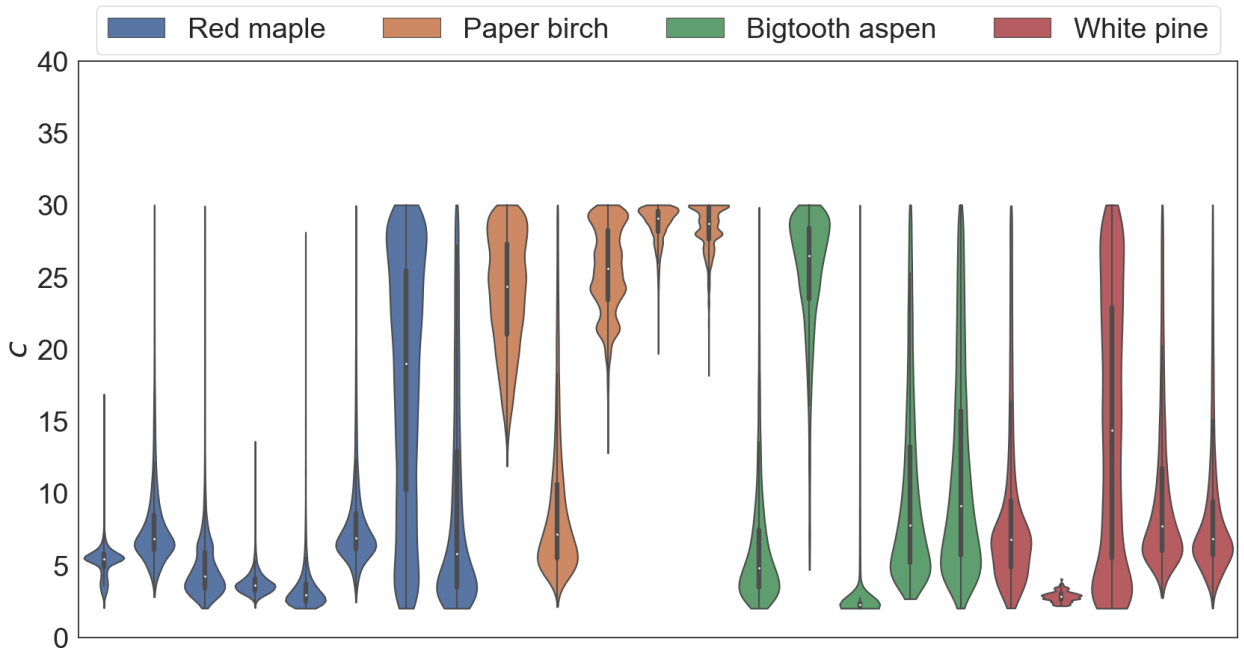

404

405 **Figure 2**. Posterior distributions of *c* (stomatal sensitivity to decreasing xylem water potential)
406 with prior distribution as Uniform [2, 30]. Each bar represents an individual tree. Color indicates
407 species: blue for red maple, yellow for paper birch, green for bigtooth aspen, and red for white
408 pine.

409 The parameter that captures stomatal sensitivity to drought, *c*, describes how quickly plants close
410 stomata in response to decreasing plant water potential. A higher value of *c* indicates an earlier
411 stomatal closure with decreasing plant water potential (Eq. 5). Fig. 2 shows that most of the
412 posterior distributions of *c* have strong positive skew with a peak near 2, the lower bound of the

support of its prior distribution. Compared with P50, almost all c estimates have a much larger variance, with the mean coefficient of variation around 0.38 (0.06 for P50). Also, for most individuals, the supports of their posterior distributions of c are not smaller than those of their prior distributions, a uniform distribution between 2 and 30. This difference in the inference uncertainty between P50 and c is mainly caused by our model having significantly less sensitivity to c than to P50.

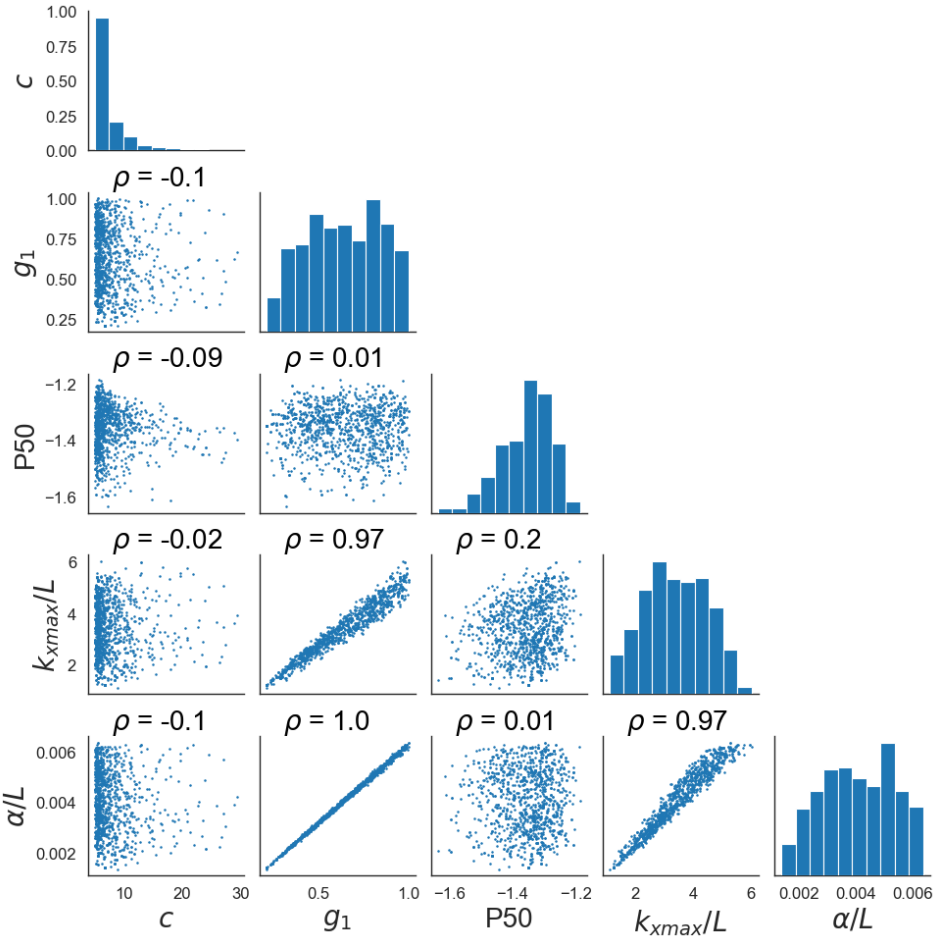

Figure 3. MCMC results of a red maple tree with the original parameters. Diagonal: posterior distributions of the fitting parameters. Off-diagonal: covariation of each pair of parameters. The Pearson correlation coefficient is denoted by ρ.

The MCMC results indicate that the values of k_{xmax}/L, α/L, and g_1 are not well constrained with our model inversion approach, due to the strong correlation among them (with correlation coefficients near 1 for almost all individuals). A typical example of this strong correlation is shown in Fig. 3 for a red maple tree. The correlation coefficients among these three parameters are near 1 in the MCMC outputs of almost all individuals. The correlation between k_{xmax}/L and α/L is understandable, as it is due to the fact that their ratio that determines how transpiration rate scales with the observed sap flow (defined in Eq. 9). However, the linear correlation between k_{xmax}/L and g_1 can only be expected when stomatal conductance g_s is high. To illustrate this, we note that our model (see Eq. 5) contains specifies a nonlinear relationship between k_{xmax}/L and g_1, which is introduced by due to the nonlinearity in the Farquhar-von Caemmerer-Berry photosynthesis model (Farquhar et al., 1980) with respect to g_s (see Eq. 5). Only when g_s takes high values does A become practically independent of g_s (i.e., photosynthesis is CO_2-saturated) and becomes concentrated around its maximum value, A_{max}, which eliminates the nonlinearity within the Farquhar model. Specifically, under this assumption, Eq. 5 can be simplified as

$$g_s \approx \frac{g_1}{\sqrt{D}} \frac{A_{max}}{c_a} e^{\left(-c f_{PLC}(\Psi_x)\right)} \tag{10}$$

Then, by combining Eqs. 8 & 10, we obtain

$$\frac{\frac{k_{xmax}}{L}}{g_1} \frac{1}{\sqrt{D}} \approx \frac{a A_{max}}{10^{-3} c_a} \frac{e^{\left(-c f_{PLC}(\Psi_x)\right)}}{\left(1 - f_{PLC}(\Psi_x)\right)(\Psi_s - \Psi_x)}, \tag{11}$$

which suggests the observed linearity between k_{xmax}/L and g_1 on the left-hand side.

The physiological meaning of the aggregated parameter $k_{xmax}/L/g_1$ can be framed in terms of differential sap flow sensitivities to soil water stress compared to atmospheric water stress. The left-hand side of Eq. 11 decreases with increasing D while its right-hand side decreases with

decreasing Ψ_x (these trends occur under value of c larger than 2, and f_{PLC} lower than 50%, which is typically applicable for our dataset). Because, $k_{xmax}/L/g_1$ controls the relative impacts of the left- vs. right-hand side of Eq. 11 on stomatal conductance g_s, $k_{xmax}/L/g_1$ can be thought of as an indicator of the relative sensitivity to plant water potential vs. vapor pressure deficit – with any given D, a higher value of $k_{xmax}/L/g_1$ results in a less negative Ψ_x at a constant stomatal conductance.

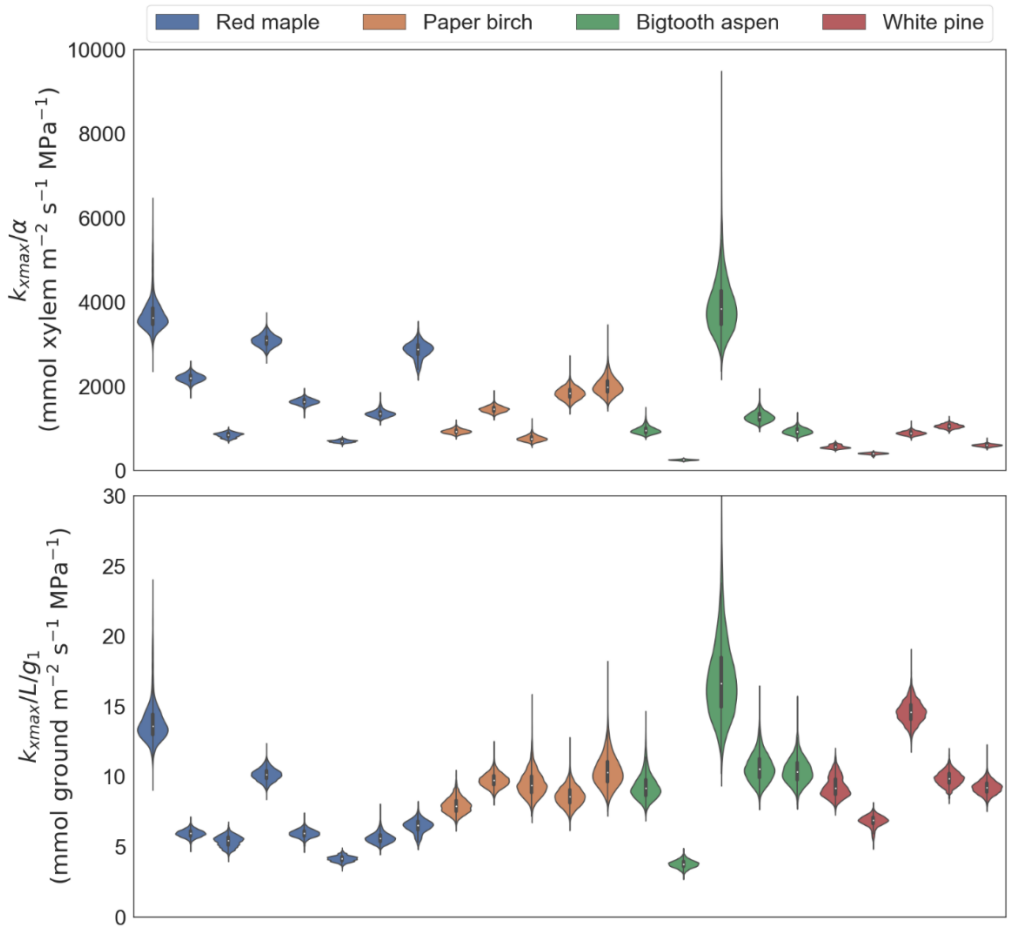

Figure 4. Posterior distributions of $k_{xmax}/L/g_1$ (lower) and k_{xmax}/α (upper) where k_{xmax} is the maximum whole-plant xylem conductance, L is the leaf area index, g_1 is inversely related to plant marginal water-use efficiency and α is the sapwood area per ground area. Color indicates species (blue: red maple; brown: paper birch; green: bigtooth aspen; red: white pine).

Unlike its two strongly correlated component parameters, k_{xmax}/L and g_1 (Fig. 3), we display our results in terms of this aggregated parameter $k_{xmax}/L/g_1$ (left hand side of Eq. 11), which is well constrained with our model inversion approach and has very low uncertainty for every individual (Fig. 4, lower panel). Similarly, the other aggregated parameter, k_{xmax}/α, which represents the maximum xylem conductance per xylem sapwood area, is also well constrained and inferred with low uncertainty (Fig. 4, upper panel). These results suggest that, in addition to a range of drought tolerance (based on results for P50; Fig. 1), these individuals also exhibit variations in their relative sensitivities to atmospheric drought (through vapor pressure deficit) or water status (through plant water potentials).

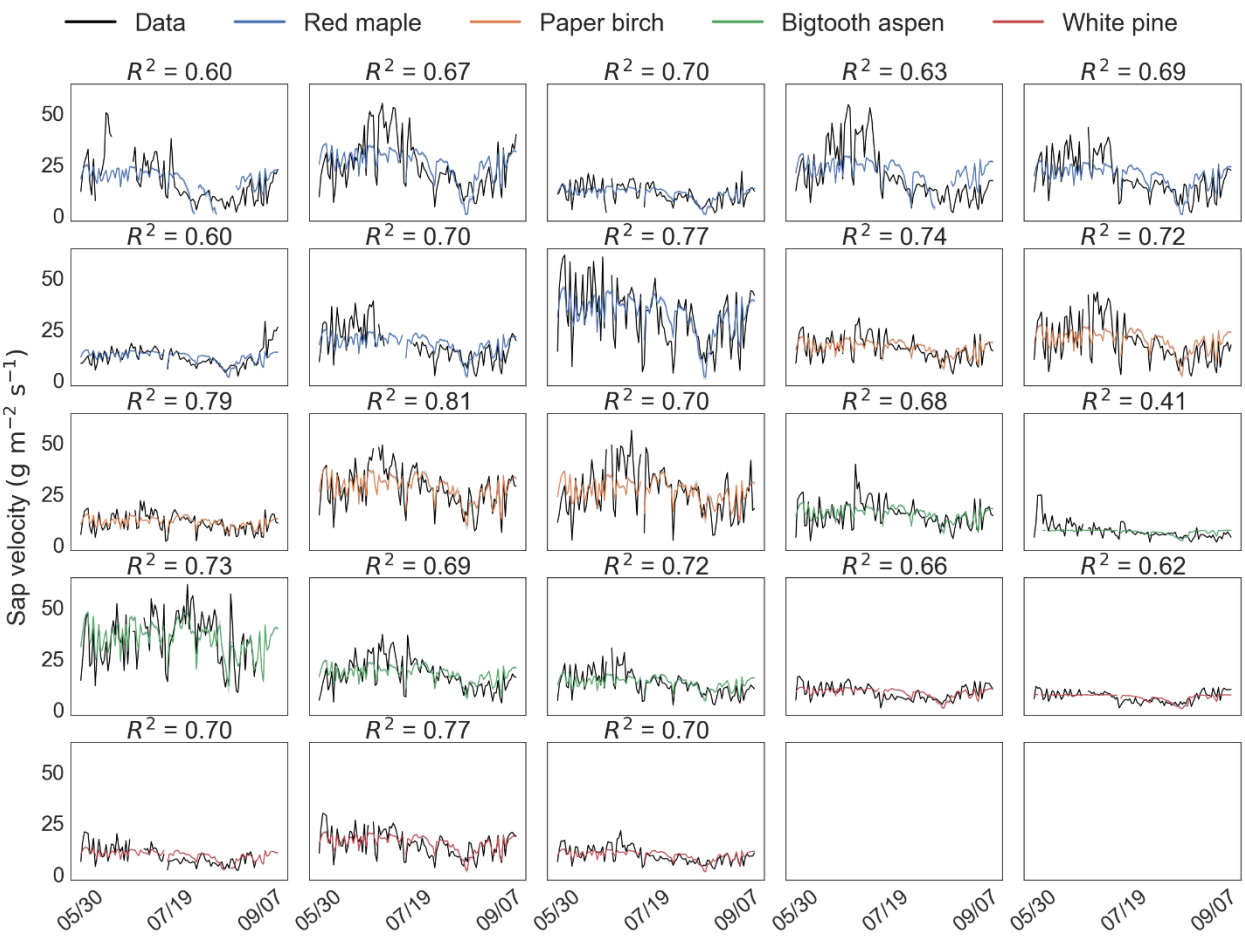

Figure 5. Estimates of sap flow. The 5th, 50th, and 95th percentiles of 1000 MCMC estimates of the sap flow time series are in close agreement with the input data (black). Color indicates species (blue: red maple; brown: paper birch; green: bigtooth aspen; red: white pine).

3.2 MCMC predictions of sap flow, plant water potential, and isohydricity

We confirm that our inferred parameters can be used to adequately capture the seasonal variation in the observed sap flow. Fig. 5 shows that the ensemble prediction matches reasonably with the observed daily average sap flow in the input sapflow data and has very low uncertainty (where the uncertainty is defined as the interval between the 5th and 95th percentiles of the ensemble prediction of sap flow; note that both the 5th and 95th percentiles of the ensemble prediction are too close to the median to be visually identified in Fig. 5). The correlation between the observed sap flow and the median of the ensemble model prediction is generally strong. The mean correlation coefficient across all individuals is 0.69. However, Fig. 5 also shows that our approach seems to be only able to capture the overall seasonal trend in the observed dynamics of sap flow, but not the oscillation on finer (e.g., daily) time scales.The inferred parameters can also be used to capture inter- and intraspecies isohydricity variability through σ (Figure 6a), defined by the decline in plant water potential with soil water potential (Figure 6b). The paper birch and bigtooth aspen allow Ψ_x to decline faster with Ψ_s compared to the red maple and eastern white pine, corresponding to more anisohydric behavior consistent with previous knowledge shown in Table 1. The fits for the remaining trees (Figure S6) show much scatter near soil saturation, which is due to variability in *D*.We also tested the statistical significance of the interspecies differences in σ (Figure S8). A single factor ANOVA confirmed that the species-specific σ values are statistically different ($p = 0.014$); however, the pairwise t-tests using Tukey's HSD struggled to find significant differences between the species σ values due to the large intra-

species variability for aspen and pine (Fig. 6a). Tukey's HSD only yields a statistically significant difference between pine and birch (p = 0.022), while the difference in birch and maple (p = 0.06) and aspen and pine (p = 0.1) were above the 5% significance level (note that Tukey's HSD tends to be extremely conservative, which may lower the power of the test (Efron and Hastie, 2016)). Nevertheless, these results illustrate the importance in accounting for the intraspecies variability, as it can potentially overtake the range in interspecific variability.

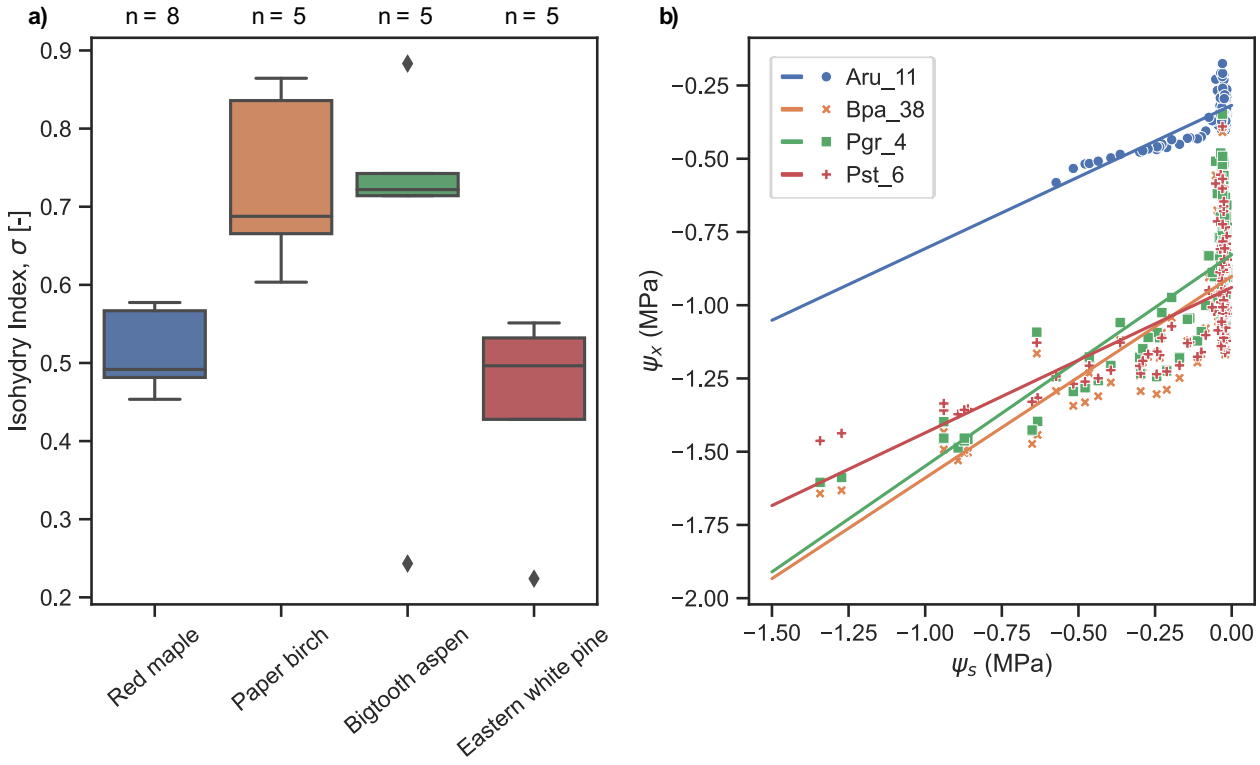

Figure 6. a) Isohydricity indices (σ) extracted from ψ_x and ψ_s values at each site. Values closer to 0 indicate isohydric and values closer to 1 indicate anisohydric behavior. **b)** Actual water potential data (dots) and fit lines used to extract σ for one site of each species. Specifically, we are showing the trees that contained the median σ for each species. The individual fits for each site are shown in Fig. S6.

3.3 Uncertainty analysis

In this subsection, we report the effects of three main contributors to the uncertainty associated with parameter estimation: 1) low parameter sensitivity, 2) measurement error, and 3) the lack of prior information on the fitting parameters. First, we examine the effects of parameter sensitivity and focus on the comparison between two parameters, plant vulnerability to embolism, P50, and *c*. In this study, they show contrasting degrees of inference uncertainty – the posterior distributions of P50 have a much smaller variance than those for *c* (Figs. 1 & 2). Our sensitivity analysis shows that this difference can be explained by the different degrees to which the model output (i.e., sap flow) is sensitive to each parameter. As shown in Fig. 7 (left panel), P50 has a much larger Sobol's total-order sensitivity index than *c* (the mean total-order index is 0.64 for P50 and 0.20 for *c*). Also, the first-order index of *c* is close to zero (about 0.015), indicating that this parameter has a very limited effect on the modeled sap flow on its own. These results confirm that our sap flow model is much more sensitive to the change in P50 than to *c*. Necessarily, this leads to a larger uncertainty in estimates of *c* relative to P50. These relative degrees of parameter sensitivity hold whether soil water potential is known or unknown: in the absence of soil water potential data, the model remains much more sensitive to P50 rather than *c* (Fig. 7, right panel).

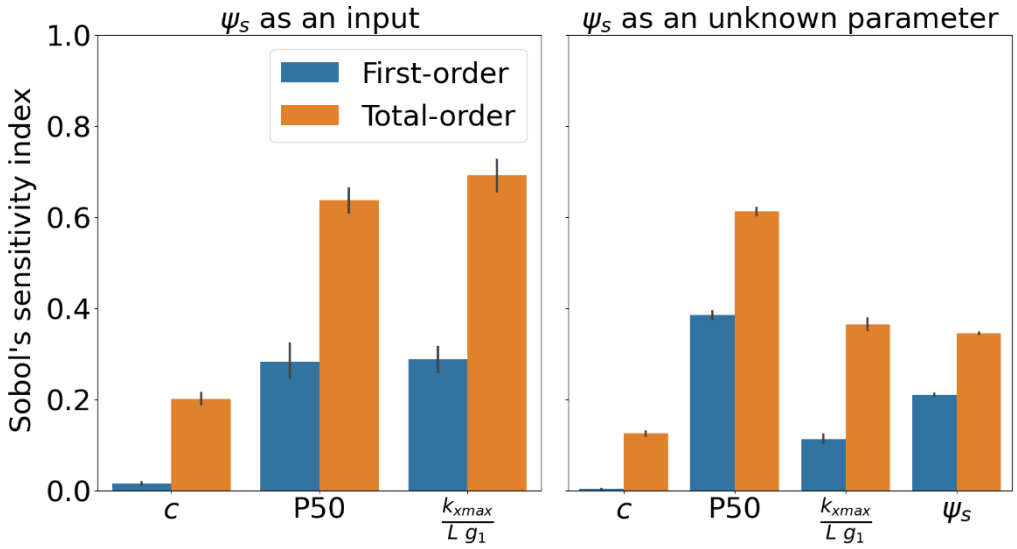

Figure 7. Sobol's first-order and total order sensitivity indices. We consider two scenarios: the soil water potential as a model input (left panel) and a fitting parameter (right panel).

We also evaluate the consequence of absent soil water potential measurements during parameter inference by inferring it as an unknown parameter. In Fig. 7 (right panel), we show that soil water potential as a model parameter is very sensitive as both its first- and total-order indices are high (its mean first- and total-order indices are 0.21 and 0.35, respectively).

We analyze the next two sources of uncertainty – measurement error and low prior knowledge – based on synthetic experiments (Section 2.4). Here, we use P50 as an example and demonstrate the effects of measurement error on its posterior distribution. Noise in sap flow data creates irregular uncertainty in P50 (Fig. S4), with no consistent trend in bias and uncertainty of the P50 estimate as the noise level increases. In contrast to noise in the sap flow data, bias in the soil water potential measurements does have large impacts on the estimated value of P50. While all the above model inversion results (Figs. 1-5) are based on the assumption of our soil water potential measurement (Section 2.1) being accurate, Fig. 8 shows that when soil water potential measurements are systematically more negative than their true values, MCMC tends to

underestimate the true synthetic value of P50, resulting in more negative P50, and vice versa.

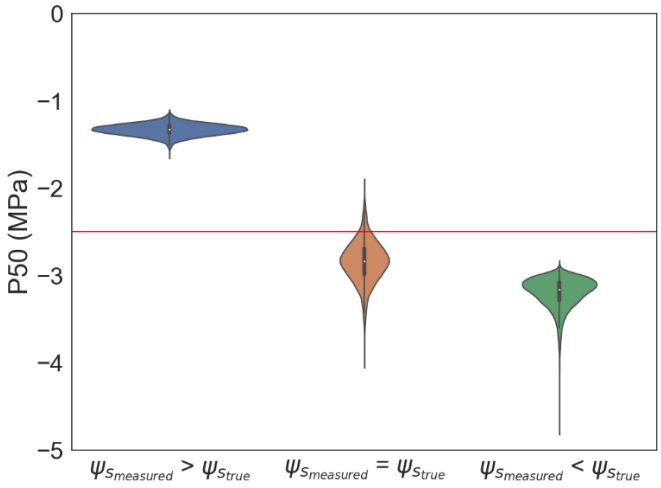

Figure 8. Posterior distributions of P50 inferred using soil water potential data at different bias levels. The horizontal line labels the prescribed synthetic truth.

Finally, the uncertainty in parameter estimation may also be attributed to the lack of detailed prior knowledge of the fitting parameter. Our analysis shows that the effect of prior knowledge on the accuracy of different parameters' estimates varies strongly with model sensitivity to that parameter. For both P50 and *c*, we evaluate the impact of prior knowledge qualitatively by comparing the posterior distribution of each parameter based on an MCMC inversion with a noninformative uniform prior with the posterior distribution using an informative truncated normal prior distribution (see Fig. 9a). In Fig. 9, we show that with more prior information (using the truncated normal distribution), the uncertainty of the *c* estimate decreases significantly. This improvement in the estimate for *c* does *not* come from making use of information contained in the data, because the posterior distribution (Fig. 9, right panel, blue) largely overlaps with the prior distribution (Fig. 9, left panel, blue). This presumably reflects the low sensitivity of *c* (c.f. Fig. 7). By contrast, more prior knowledge barely improves the estimate of P50: the two posterior distributions resulting from the uniform and truncated normal prior

distributions are similar (Fig. 9, middle panel). There is higher certainty in the P50 posterior distributions, regardless of prior knowledge, relative to *c*, because the sap flow constrains the highly sensitive P50 parameter very well (see Fig. 7). Under these circumstances, an informative prior cannot provide much additional information to reduce the uncertainty in the P50 estimate, relative to a flat prior.

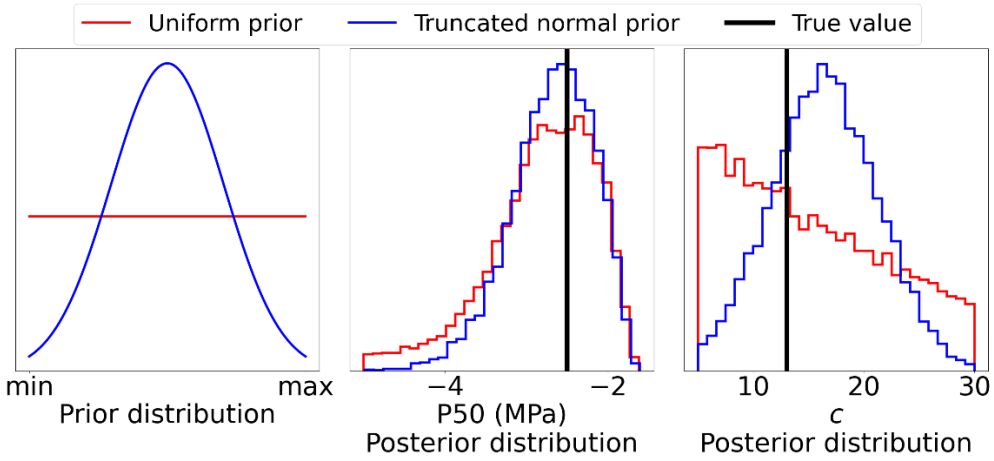

Figure 9. Prior distributions (left) and the corresponding posterior distributions of P50 (middle) and *c* (right). Color indicates the type of prior distribution: red for uniform distribution and blue for truncated normal distribution. The vertical black lines in the middle and right panels indicate the true values of P50 and *c*, respectively.

4 Discussion

4.1 MCMC model inversion reliably predicts seasonal sap flow variations

With the use of a simple model in combination with sap flow, soil water potential, and atmospheric data, we have demonstrated that an MCMC model inversion approach is able to predict seasonal sap flow variations across a range of environmental conditions (e.g., solar irradiance, vapor pressure deficit, temperature, and soil water potential; Figure 5). This ability to

capture seasonal sap flow variations is an indication that the simple model used is realistic enough to represent complex plant behaviors. It also supports the assumption of strong coordination between stomatal conductance and plant water potential (Anderegg et al., 2017) embedded within Eq. 5, which results in stomatal closure occurring substantially earlier than any significant hydraulic impairment (Fig. S5), as commonly observed (e.g., Bartlett et al., 2016; Martin-StPaul et al., 2017).

4.2 Whole-plant hydraulic parameters inferred through model inversion

The accuracy with which the MCMC approach predicted sap flow variations (Figure 5) suggest that hydraulic parameters (Figures 1-4) can be reliably estimated. Our MCMC model inversion approach provides a means to infer whole-plant parameters values without scaling leaf or branch-level trait measurements. Typically, a plant is segmented into roots, xylem, and leaf for measurement (Sperry et al., 1998), requiring time consuming measurements in each segment (e.g., bench dehydration of a branch to find P50) and questions as to how well these local measurements can be representative of the whole-plant response. Instead, by using a model that captures whole-plant level sap flow as a starting point, the inferred parameters are directly applicable for whole-plant predictions (subject to the assumption that sap flow measurements are taken on the main stem, and with negligible effects of xylem capacitance, which is assumed by state-of-the-art terrestrial biosphere models (Kennedy et al., 2019; Eller et al., 2020; Sabot et al., 2020)).These whole-plant parameter values are particularly useful to parameterize PHMs that do not separate branches from other plant components. For the same reason, values derived from this approach may be difficult to compare to current measurements. For example, our analysis (Supporting Information) shows that the effective whole-plant P50 is likely to be lower than P50 in the roots and higher than P50 in the stems closer to the canopy. This is consistent with our

results (Fig. 1) that show higher values of whole-plant inferred P50 than measured leaf or branch P50 for red maple and, to a lesser extent, paper birch. It is also consistent with the P50 values inferred from eddy covariance by MCMC in Liu et al (2020), for which in situ measurements of branch P50 were generally higher than the inferred whole-plant values.

4.3 Intra- and inter- specific variations in plant water use strategies

The low uncertainty around most inferred parameters (except for *c*) allows for the quantification of inter- and intraspecific variability in hydraulic traits. Trait variability has been observed in P50 and other hydraulic traits measured at the stem and branch levels (Anderegg et al., 2018; Bartlett et al., 2014; Trugman et al., 2019). Our analysis provides a preliminary look at whole-plant trait variability among and within four tree species (Figs. 1, 2, & 4) that can be used to improve predictions of ecosystem scale fluxes. The low intraspecific variability in P50 for all species (Fig. 1) may be explained by the fact that all individuals grow on the same site and by our assumption that all trees experience the same environment. Further work must be done to ensure that sap flux measurements of individuals are representative of the species in the ecosystem and evaluate the extent to which these parameter values may vary across sites.

The prediction of plant water potential based on inferred traits allowed us to characterize the water use strategies of each individual using an isohydricity index (Figure 6), which confirmed prior knowledge of aspen and maple at the site (Table 1), while providing new insights on birch and pine. More importantly, our analysis highlighted the intraspecies variability of plant water-use strategy that emerges from hydraulic trait variability. In particular, aspen and pine contained one very isohydric outlier each (site Pgr-27 and site Pst-14 shown in Figure S7) relative to the other four trees in each species group. Although the MCMC inversion for these two individuals yielded relatively insensitive stomata (low *c*), their low xylem conductance per sapwood area

(k_{xmax}/α) caused enhanced stomatal closure and relatively stable plant water potential under soil water stress (see Figure S7). To the best of our knowledge, there were no extenuating circumstances (e.g., mortality, differing soil water conditions) or noticeable measurement errors that could explain these outliers. Therefore, barring significant deficiencies in our MCMC inversion, this result reinforces the importance of understanding intra-species variability of hydraulic traits, especially to understand plant response to water stress.

4.4 Reducing uncertainties via additional soil and plant water potential data

The MCMC results also help inform the collection of new soil or plant hydraulic data and extract additional information from existing datasets. For example, the results show that measured soil water potential at sites where sap flow measurements are taken is essential for reliable parameter inference (Fig. 7) and its accuracy has a great impact on the bias in parameter inference (Fig. 8). Therefore, study sites should be set up with at least a single profile of soil water potential to help interpret and extend the utility of sap flow measurements. Systematic biases in soil water potential measurement can be almost certainly expected from the use of a site-wide soil water potential measurement. This bias has been shown to strongly increase the uncertainty in hydraulic model prediction (e.g., soil water budget and transpiration) (Baroni et al., 2017; Zhu et al., 2018). In Chirico et al., (2010), the soil water potential bias is introduced specifically by the parameter uncertainty in pedotransfer functions (which converts soil moisture into soil water potential). The lack of continuously measured soil water potential data at many monitoring sites remains a challenge for leveraging flux data to advance our understanding of land-atmosphere interactions (Novick et al., 2019).

Alternatively, measurements of soil moisture, which are much more widely available, can be converted to soil water potentials using measured soil water retention curves, as in this study.

633 However, this conversion can be challenging in complex and heterogeneous soil substrates and
634 must be accurate enough to ensure the quality of hydraulic model predictions (Chirico et al.,
635 2010).

636 ### 4.5 Implications of limitations in model structure

637 While P50, $k_{xmax}/L/g_1$, k_{xmax}/α are well-constrained at this site and for these species, estimates of
638 the stomatal sensitivity to drought (i.e., c) are much more uncertain for almost all individuals in
639 the UMBS dataset. This uncertainty is mainly driven by the lack of sensitivity to c of the sap
640 flow model (Fig. 7). This means that estimation of c cannot be further improved by inversion of
641 the sap flux model. Alternative model structures could be considered, but the adoption of
642 alternative models is constrained by the data available to serve as model inputs and outputs.
643 Some datasets could potentially better constrain some model parameters than others (Luo et al.,
644 2009), because these datasets might be more compatible with models that are sensitive to
645 specific parameters. Thus, while we have shown the value of sap flux data for inferring P50, its
646 utility for inferring stomatal closure parameters may be more limited unless coupled to additional
647 measurements that are not available in this study (e.g., plant water potential).

648 ## 5 Conclusions

649 Here, we have demonstrated that PHM hydraulic parameters can be inferred at the individual
650 level using a MCMC inversion approach using measured sap flow. Reliable and simultaneous
651 inference of multiple hydraulic model parameters has great potential to assist model
652 parametrization, which remains a major impediment to the adoption of PHMs (Feng, 2020;
653 Paschalis et al., 2020; Sloan et al. 2021). The inferred hydraulic traits – including the whole-
654 plant effective embolism vulnerability and maximum xylem conductance – are subject to a

number of uncertainties related to model structure and input data availability but capture well the inter and intra-specific variability in plant water use and hydraulic vulnerability.Inferring plant hydraulic traits using sap flow data based on MCMC relies on accurate measurement of soil water potential with minimum bias, suggesting that measurements of soil water potential could be usefully incorporated into ecohydrological and ecophysiological observation campaigns for this purpose. While soil moisture data is commonly used as a substitute in practice, the conversion of soil moisture into soil water potential can be particularly challenging in any site with complex belowground structure. Furthermore, the accuracy of the model predictions can be further enhanced by comparison to plant water potential data. We conclude that although the MCMC inversion approach does not estimate all hydraulic parameters equally well, it is possible to infer some plant hydraulic traits using readily available indirect measurements (e.g., sap flow and meteorological data) with low uncertainty, and thus to augment time- and labor-intensive direct measurements.

Acknowledgements

Funding for US-UMB AmeriFlux core site was provided by the U.S. Department of Energy's Office of Science. Sap flux observations in US-UMB were funded by NSF award 1521238. We thank Jesse Hahm and Yanlan Liu for insightful discussions and suggestions during the course of this project. Special thanks are also due to the Minnesota Supercomputer Institute (MSI) computing facilities. A.M. was supported by the US Department of Energy TES grant DE-SC0020116 and the US National Science Foundation EAR CAREER award #2046768. A.G.K. was supported by NSF DEB award 1942133 and by NASA Carbon Cycle Science grant 80NSSC21K1712. X.F. and B.S. were supported by NSF DEB award 2045610. G.B. was supported by BARD award IS-5304-20.

Data Availability Statement

All data used in this study are publicly available. Meteorological, soil moisture and surface fluxes data are available through Ameriflux, site-ID US-UMB (Gough et al. 1999) https://ameriflux.lbl.gov/sites/siteinfo/US-UMB. The sap flux dataset is available from the SAPFLUXNET (Poyatos et al., 2020, 2016) https://zenodo.org/record/3971689#.YlQpeOjMKUk.

References

Allen, C.D., Macalady, A.K., Chenchouni, H., Bachelet, D., McDowell, N., Vennetier, M., Kitzberger, T., Rigling, A., Breshears, D.D., Hogg, E.H. (Ted), Gonzalez, P., Fensham, R., Zhang, Z., Castro, J., Demidova, N., Lim, J.-H., Allard, G., Running, S.W., Semerci, A., Cobb, N., 2010. A global overview of drought and heat-induced tree mortality reveals emerging climate change risks for forests. Forest Ecology and Management, Adaptation of Forests and Forest Management to Changing Climate 259, 660–684. https://doi.org/10.1016/j.foreco.2009.09.001

Anderegg, W. R. L., Venturas, M. D., 2020. Plant hydraulics play a critical role in Earth system fluxes. New Phytologist, 4. https://doi.org/10.1111/nph.16548

Anderegg, W.R.L., Wolf, A., Arango-Velez, A., Choat, B., Chmura, D.J., Jansen, S., Kolb, T., Li, S., Meinzer, F., Pita, P., Dios, V.R. de, Sperry, J.S., Wolfe, B.T., Pacala, S., 2017. Plant water potential improves prediction of empirical stomatal models. PLOS ONE 12, e0185481. https://doi.org/10.1371/journal.pone.0185481

Anderegg, L.D.L., Berner, L.T., Badgley, G., Sethi, M.L., Law, B.E., HilleRisLambers, J., 2018. Within-species patterns challenge our understanding of the leaf economics spectrum. Ecology Letters 21, 734–744. https://doi.org/10.1111/ele.12945

Anderegg, W.R.L., 2015. Spatial and temporal variation in plant hydraulic traits and their relevance for climate change impacts on vegetation. New Phytologist 205, 1008–1014. https://doi.org/10.1111/nph.12907

Baroni, G., Zink, M., Kumar, R., Samaniego, L., Attinger, S., 2017. Effects of uncertainty in soil properties on simulated hydrological states and fluxes at different spatio-temporal scales. Hydrology and Earth System Sciences 21, 2301–2320. https://doi.org/10.5194/hess-21-2301-2017

Bartlett, M.K., Klein, T., Jansen, S., Choat, B., Sack, L., 2016. The correlations and sequence of plant stomatal, hydraulic, and wilting responses to drought. PNAS 113, 13098–13103. https://doi.org/10.1073/pnas.1604088113

Bartlett, M.K., Zhang, Y., Kreidler, N., Sun, S., Ardy, R., Cao, K., Sack, L., 2014. Global analysis of plasticity in turgor loss point, a key drought tolerance trait. Ecology Letters 17, 1580–1590. https://doi.org/10.1111/ele.12374

Belluau, M., Shipley, B., 2018. Linking hard and soft traits: Physiology, morphology and anatomy interact to determine habitat affinities to soil water availability in herbaceous dicots. PLOS ONE 13, e0193130. https://doi.org/10.1371/journal.pone.0193130

Blackman, C.J., Creek, D., Maier, C., Aspinwall, M.J., Drake, J.E., Pfautsch, S., O'Grady, A., Delzon, S., Medlyn, B.E., Tissue, D.T., Choat, B., 2019. Drought response strategies and hydraulic traits contribute to mechanistic understanding of plant dry-down to hydraulic failure. Tree Physiology 39, 910–924. https://doi.org/10.1093/treephys/tpz016

Bonan, G.B., 2008. Forests and Climate Change: Forcings, Feedbacks, and the Climate Benefits of Forests. Science 320, 1444–1449. https://doi.org/10.1126/science.1155121

723 Bonan, G.B., Williams, M., Fisher, R.A., Oleson, K.W., 2014. Modeling stomatal conductance in
724 the earth system: linking leaf water-use efficiency and water transport along the soil–
725 plant–atmosphere continuum. Geosci. Model Dev. 7, 2193–2222.
726 https://doi.org/10.5194/gmd-7-2193-2014
727 Brodribb, T.J., Cochard, H., 2009. Hydraulic Failure Defines the Recovery and Point of Death in
728 Water-Stressed Conifers. Plant Physiology 149, 575–584.
729 https://doi.org/10.1104/pp.108.129783
730 Chirico, G.B., Medina, H., Romano, N., 2010. Functional evaluation of PTF prediction
731 uncertainty: An application at hillslope scale. Geoderma 155, 193–202.
732 https://doi.org/10.1016/j.geoderma.2009.06.008
733 Choat, B., Jansen, S., Brodribb, T.J., Cochard, H., Delzon, S., Bhaskar, R., Bucci, S.J., Feild,
734 T.S., Gleason, S.M., Hacke, U.G., Jacobsen, A.L., Lens, F., Maherali, H., Martínez-
735 Vilalta, J., Mayr, S., Mencuccini, M., Mitchell, P.J., Nardini, A., Pittermann, J., Pratt,
736 R.B., Sperry, J.S., Westoby, M., Wright, I.J., Zanne, A.E., 2012. Global convergence in
737 the vulnerability of forests to drought. Nature 491, 752–755.
738 https://doi.org/10.1038/nature11688
739 Christoffersen, B. O., Gloor, M., Fauset, S., Fyllas, N. M., Galbraith, D. R., Baker, T. R., …
740 Meir, P., 2016. Linking hydraulic traits to tropical forest function in a size-structured and
741 trait-driven model (TFS v.1-Hydro). Geoscientific Model Development, 9(11), 4227–
742 4255. https://doi.org/10.5194/gmd-9-4227-2016
743 Dai, A., 2011. Drought under global warming: a review. WIREs Climate Change 2, 45–65.
744 https://doi.org/10.1002/wcc.81

745 Deacon, N.J., Grossman, J.J., Cavender-Bares, J., 2019. Drought and freezing vulnerability of
746 the isolated hybrid aspen Populus x smithii relative to its parental species, P. tremuloides
747 and P. grandidentata. Ecology and Evolution 9, 8062–8074.
748 https://doi.org/10.1002/ece3.5364
749 De Kauwe, M.G., Medlyn, B.E., Ukkola, A.M., Mu, M., Sabot, M.E.B., Pitman, A.J., Meir, P.,
750 Cernusak, L.A., Rifai, S.W., Choat, B., Tissue, D.T., Blackman, C.J., Li, X., Roderick,
751 M., Briggs, P.R., 2020. Identifying areas at risk of drought-induced tree mortality across
752 South-Eastern Australia. Global Change Biology 26, 5716–5733.
753 https://doi.org/10.1111/gcb.15215

754 De Kauwe, M. G., Zhou, S.-X., Medlyn, B. E., Pitman, A. J., Wang, Y.-P., Duursma, R. A.,
755 Prentice, I. C., 2015. Do land surface models need to include differential plant species
756 responses to drought? Examining model predictions across a mesic-xeric gradient in
757 Europe. *Biogeosciences*, *12*, 7503–7518. https://doi.org/10.5194/bg-12-7503-2015

758 Efron, B., & Hastie, T. (2016). Computer age statistical inference: Algorithms, evidence, and
759 data science. Computer Age Statistical Inference: Algorithms, Evidence, and Data
760 Science. https://doi.org/10.1017/CBO9781316576533

761 Eller, C.B., Rowland, L., Mencuccini, M., Rosas, T., Williams, K., Harper, A., Medlyn, B.E.,
762 Wagner, Y., Klein, T., Teodoro, G.S., Oliveira, R.S., Matos, I.S., Rosado, B.H.P., Fuchs,
763 K., Wohlfahrt, G., Montagnani, L., Meir, P., Sitch, S., Cox, P.M., 2020. Stomatal
764 optimization based on xylem hydraulics (SOX) improves land surface model simulation
765 of vegetation responses to climate. New Phytologist 226, 1622–1637.
766 https://doi.org/10.1111/nph.16419

767 Farquhar, G.D., Caemmerer, S. von, Berry, J.A., 1980. A biochemical model of photosynthetic
768 CO2 assimilation in leaves of C3 species. Planta 149, 78–90.
769 https://doi.org/10.1007/BF00386231
770 Feng, X., 2020. Marching in step: The importance of matching model complexity to data
771 availability in terrestrial biosphere models. Global Change Biology 26, 3190–3192.
772 https://doi.org/10.1111/gcb.15090
773 Feng, X., Ackerly, D.D., Dawson, T.E., Manzoni, S., McLaughlin, B., Skelton, R.P., Vico, G.,
774 Weitz, A.P., Thompson, S.E., 2019. Beyond isohydricity: The role of environmental
775 variability in determining plant drought responses. Plant Cell Environ 42, 1104–1111.
776 https://doi.org/10.1111/pce.13486
777 Field, C.B., Barros, V., Stocker, T.F., Dahe, Q. (Eds.), 2012. Managing the Risks of Extreme
778 Events and Disasters to Advance Climate Change Adaptation: Special Report of the
779 Intergovernmental Panel on Climate Change. Cambridge University Press, Cambridge.
780 https://doi.org/10.1017/CBO9781139177245
781 Gough, C.M., Hardiman, B.S., Nave, L.E., Bohrer, G., Maurer, K.D., Vogel, C.S., Nadelhoffer,
782 K.J., Curtis, P.S., 2013. Sustained carbon uptake and storage following moderate
783 disturbance in a Great Lakes forest. Ecological Applications 23, 1202–1215.
784 https://doi.org/10.1890/12-1554.1
785 Gough, C.M., Bohrer, G., Curtis, P.S., 1999. AmeriFlux US-UMB Univ. of Mich. Biological
786 Station, Dataset. https://doi.org/10.17190/AMF/1246107
787 He, L., Ivanov, V.Y., Bohrer, G., Maurer, K.D., Vogel, C.S., Moghaddam, M., 2014. Effects of
788 fine-scale soil moisture and canopy heterogeneity on energy and water fluxes in a

northern temperate mixed forest. Agricultural and Forest Meteorology 184, 243–256. https://doi.org/10.1016/j.agrformet.2013.10.006

He, L., Ivanov, V.Y., Bohrer, G., Thomsen, J.E., Vogel, C.S., Moghaddam, M., 2013. Temporal dynamics of soil moisture in a northern temperate mixed successional forest after a prescribed intermediate disturbance. Agricultural and Forest Meteorology 180, 22–33. https://doi.org/10.1016/j.agrformet.2013.04.014

Hou, Z., Rubin, Y., 2005. On minimum relative entropy concepts and prior compatibility issues in vadose zone inverse and forward modeling. Water Resources Research 41. https://doi.org/10.1029/2005WR004082

Kannenberg, S. A., Guo, J. S., Novick, K. A., Anderegg, W. R. L., Feng, X., Kennedy, D., et al. (2021). Opportunities, challenges and pitfalls in characterizing plant water-use strategies. Functional Ecology, n/a(n/a). https://doi.org/10.1111/1365-2435.13945

Kattge, J., Bönisch, G., Díaz, S., Lavorel, S., Prentice, I.C., Leadley, P., Tautenhahn, S., Werner, G.D.A., Aakala, T., Abedi, M., Acosta, A.T.R., Adamidis, G.C., Adamson, K., Aiba, M., Albert, C.H., Alcántara, J.M., C, C.A., Aleixo, I., Ali, H., Amiaud, B., Ammer, C., Amoroso, M.M., Anand, M., Anderson, C., Anten, N., Antos, J., Apgaua, D.M.G., Ashman, T.-L., Asmara, D.H., Asner, G.P., Aspinwall, M., Atkin, O., Aubin, I., Baastrup-Spohr, L., Bahalkeh, K., Bahn, M., Baker, T., Baker, W.J., Bakker, J.P., Baldocchi, D., Baltzer, J., Banerjee, A., Baranger, A., Barlow, J., Barneche, D.R., Baruch, Z., Bastianelli, D., Battles, J., Bauerle, W., Bauters, M., Bazzato, E., Beckmann, M., Beeckman, H., Beierkuhnlein, C., Bekker, R., Belfry, G., Belluau, M., Beloiu, M., Benavides, R., Benomar, L., Berdugo-Lattke, M.L., Berenguer, E., Bergamin, R., Bergmann, J., Carlucci, M.B., Berner, L., Bernhardt-Römermann, M., Bigler, C.,

Bjorkman, A.D., Blackman, C., Blanco, C., Blonder, B., Blumenthal, D., Bocanegra-González, K.T., Boeckx, P., Bohlman, S., Böhning-Gaese, K., Boisvert-Marsh, L., Bond, W., Bond-Lamberty, B., Boom, A., Boonman, C.C.F., Bordin, K., Boughton, E.H., Boukili, V., Bowman, D.M.J.S., Bravo, S., Brendel, M.R., Broadley, M.R., Brown, K.A., Bruelheide, H., Brumnich, F., Bruun, H.H., Bruy, D., Buchanan, S.W., Bucher, S.F., Buchmann, N., Buitenwerf, R., Bunker, D.E., Bürger, J., Burrascano, S., Burslem, D.F.R.P., Butterfield, B.J., Byun, C., Marques, M., Scalon, M.C., Caccianiga, M., Cadotte, M., Cailleret, M., Camac, J., Camarero, J.J., Campany, C., Campetella, G., Campos, J.A., Cano-Arboleda, L., Canullo, R., Carbognani, M., Carvalho, F., Casanoves, F., Castagneyrol, B., Catford, J.A., Cavender-Bares, J., Cerabolini, B.E.L., Cervellini, M., Chacón-Madrigal, E., Chapin, K., Chapin, F.S., Chelli, S., Chen, S.-C., Chen, A., Cherubini, P., Chianucci, F., Choat, B., Chung, K.-S., Chytrý, M., Ciccarelli, D., Coll, L., Collins, C.G., Conti, L., Coomes, D., Cornelissen, J.H.C., Cornwell, W.K., Corona, P., Coyea, M., Craine, J., Craven, D., Cromsigt, J.P.G.M., Csecserits, A., Cufar, K., Cuntz, M., Silva, A.C. da, Dahlin, K.M., Dainese, M., Dalke, I., Fratte, M.D., Dang-Le, A.T., Danihelka, J., Dannoura, M., Dawson, S., Beer, A.J. de, Frutos, A.D., Long, J.R.D., Dechant, B., Delagrange, S., Delpierre, N., Derroire, G., Dias, A.S., Diaz-Toribio, M.H., Dimitrakopoulos, P.G., Dobrowolski, M., Doktor, D., Dřevojan, P., Dong, N., Dransfield, J., Dressler, S., Duarte, L., Ducouret, E., Dullinger, S., Durka, W., Duursma, R., Dymova, O., E-Vojtkó, A., Eckstein, R.L., Ejtehadi, H., Elser, J., Emilio, T., Engemann, K., Erfanian, M.B., Erfmeier, A., Esquivel-Muelbert, A., Esser, G., Estiarte, M., Domingues, T.F., Fagan, W.F., Fagúndez, J., Falster, D.S., Fan, Y., Fang, J., Farris, E., Fazlioglu, F., Feng, Y., Fernandez-Mendez, F., Ferrara, C., Ferreira, J., Fidelis, A.,

Finegan, B., Firn, J., Flowers, T.J., Flynn, D.F.B., Fontana, V., Forey, E., Forgiarini, C., François, L., Frangipani, M., Frank, D., Frenette-Dussault, C., Freschet, G.T., Fry, E.L., Fyllas, N.M., Mazzochini, G.G., Gachet, S., Gallagher, R., Ganade, G., Ganga, F., García-Palacios, P., Gargaglione, V., Garnier, E., Garrido, J.L., Gasper, A.L. de, Gea-Izquierdo, G., Gibson, D., Gillison, A.N., Giroldo, A., Glasenhardt, M.-C., Gleason, S., Gliesch, M., Goldberg, E., Göldel, B., Gonzalez-Akre, E., Gonzalez-Andujar, J.L., González-Melo, A., González-Robles, A., Graae, B.J., Granda, E., Graves, S., Green, W.A., Gregor, T., Gross, N., Guerin, G.R., Günther, A., Gutiérrez, A.G., Haddock, L., Haines, A., Hall, J., Hambuckers, A., Han, W., Harrison, S.P., Hattingh, W., Hawes, J.E., He, T., He, P., Heberling, J.M., Helm, A., Hempel, S., Hentschel, J., Hérault, B., Hereş, A.-M., Herz, K., Heuertz, M., Hickler, T., Hietz, P., Higuchi, P., Hipp, A.L., Hirons, A., Hock, M., Hogan, J.A., Holl, K., Honnay, O., Hornstein, D., Hou, E., Hough-Snee, N., Hovstad, K.A., Ichie, T., Igić, B., Illa, E., Isaac, M., Ishihara, M., Ivanov, L., Ivanova, L., Iversen, C.M., Izquierdo, J., Jackson, R.B., Jackson, B., Jactel, H., Jagodzinski, A.M., Jandt, U., Jansen, S., Jenkins, T., Jentsch, A., Jespersen, J.R.P., Jiang, G.-F., Johansen, J.L., Johnson, D., Jokela, E.J., Joly, C.A., Jordan, G.J., Joseph, G.S., Junaedi, D., Junker, R.R., Justes, E., Kabzems, R., Kane, J., Kaplan, Z., Kattenborn, T., Kavelenova, L., Kearsley, E., Kempel, A., Kenzo, T., Kerkhoff, A., Khalil, M.I., Kinlock, N.L., Kissling, W.D., Kitajima, K., Kitzberger, T., Kjøller, R., Klein, T., Kleyer, M., Klimešová, J., Klipel, J., Kloeppel, B., Klotz, S., Knops, J.M.H., Kohyama, T., Koike, F., Kollmann, J., Komac, B., Komatsu, K., König, C., Kraft, N.J.B., Kramer, K., Kreft, H., Kühn, I., Kumarathunge, D., Kuppler, J., Kurokawa, H., Kurosawa, Y., Kuyah, S., Laclau, J.-P., Lafleur, B., Lallai, E., Lamb, E., Lamprecht, A., Larkin, D.J., Laughlin, D., Bagousse-

Pinguet, Y.L., Maire, G. le, Roux, P.C. le, Roux, E. le, Lee, T., Lens, F., Lewis, S.L., Lhotsky, B., Li, Y., Li, X., Lichstein, J.W., Liebergesell, M., Lim, J.Y., Lin, Y.-S., Linares, J.C., Liu, C., Liu, D., Liu, U., Livingstone, S., Llusià, J., Lohbeck, M., López-García, Á., Lopez-Gonzalez, G., Lososová, Z., Louault, F., Lukács, B.A., Lukeš, P., Luo, Y., Lussu, M., Ma, S., Pereira, C.M.R., Mack, M., Maire, V., Mäkelä, A., Mäkinen, H., Malhado, A.C.M., Mallik, A., Manning, P., Manzoni, S., Marchetti, Z., Marchino, L., Marcilio-Silva, V., Marcon, E., Marignani, M., Markesteijn, L., Martin, A., Martínez-Garza, C., Martínez-Vilalta, J., Mašková, T., Mason, K., Mason, N., Massad, T.J., Masse, J., Mayrose, I., McCarthy, J., McCormack, M.L., McCulloh, K., McFadden, I.R., McGill, B.J., McPartland, M.Y., Medeiros, J.S., Medlyn, B., Meerts, P., Mehrabi, Z., Meir, P., Melo, F.P.L., Mencuccini, M., Meredieu, C., Messier, J., Mészáros, I., Metsaranta, J., Michaletz, S.T., Michelaki, C., Migalina, S., Milla, R., Miller, J.E.D., Minden, V., Ming, R., Mokany, K., Moles, A.T., Molnár, A., Molofsky, J., Molz, M., Montgomery, R.A., Monty, A., Moravcová, L., Moreno-Martínez, A., Moretti, M., Mori, A.S., Mori, S., Morris, D., Morrison, J., Mucina, L., Mueller, S., Muir, C.D., Müller, S.C., Munoz, F., Myers-Smith, I.H., Myster, R.W., Nagano, M., Naidu, S., Narayanan, A., Natesan, B., Negoita, L., Nelson, A.S., Neuschulz, E.L., Ni, J., Niedrist, G., Nieto, J., Niinemets, Ü., Nolan, R., Nottebrock, H., Nouvellon, Y., Novakovskiy, A., Nystuen, K.O., O'Grady, A., O'Hara, K., O'Reilly-Nugent, A., Oakley, S., Oberhuber, W., Ohtsuka, T., Oliveira, R., Öllerer, K., Olson, M.E., Onipchenko, V., Onoda, Y., Onstein, R.E., Ordonez, J.C., Osada, N., Ostonen, I., Ottaviani, G., Otto, S., Overbeck, G.E., Ozinga, W.A., Pahl, A.T., Paine, C.E.T., Pakeman, R.J., Papageorgiou, A.C., Parfionova, E., Pärtel, M., Patacca, M., Paula, S., Paule, J., Pauli, H., Pausas, J.G., Peco, B., Penuelas, J., Perea, A., Peri,

P.L., Petisco-Souza, A.C., Petraglia, A., Petritan, A.M., Phillips, O.L., Pierce, S., Pillar, V.D., Pisek, J., Pomogaybin, A., Poorter, H., Portsmuth, A., Poschlod, P., Potvin, C., Pounds, D., Powell, A.S., Power, S.A., Prinzing, A., Puglielli, G., Pyšek, P., Raevel, V., Rammig, A., Ransijn, J., Ray, C.A., Reich, P.B., Reichstein, M., Reid, D.E.B., Réjou-Méchain, M., Dios, V.R. de, Ribeiro, S., Richardson, S., Riibak, K., Rillig, M.C., Riviera, F., Robert, E.M.R., Roberts, S., Robroek, B., Roddy, A., Rodrigues, A.V., Rogers, A., Rollinson, E., Rolo, V., Römermann, C., Ronzhina, D., Roscher, C., Rosell, J.A., Rosenfield, M.F., Rossi, C., Roy, D.B., Royer-Tardif, S., Rüger, N., Ruiz-Peinado, R., Rumpf, S.B., Rusch, G.M., Ryo, M., Sack, L., Saldaña, A., Salgado-Negret, B., Salguero-Gomez, R., Santa-Regina, I., Santacruz-García, A.C., Santos, J., Sardans, J., Schamp, B., Scherer-Lorenzen, M., Schleuning, M., Schmid, B., Schmidt, M., Schmitt, S., Schneider, J.V., Schowanek, S.D., Schrader, J., Schrodt, F., Schuldt, B., Schurr, F., Garvizu, G.S., Semchenko, M., Seymour, C., Sfair, J.C., Sharpe, J.M., Sheppard, C.S., Sheremetiev, S., Shiodera, S., Shipley, B., Shovon, T.A., Siebenkäs, A., Sierra, C., Silva, V., Silva, M., Sitzia, T., Sjöman, H., Slot, M., Smith, N.G., Sodhi, D., Soltis, P., Soltis, D., Somers, B., Sonnier, G., Sørensen, M.V., Sosinski, E.E., Soudzilovskaia, N.A., Souza, A.F., Spasojevic, M., Sperandii, M.G., Stan, A.B., Stegen, J., Steinbauer, K., Stephan, J.G., Sterck, F., Stojanovic, D.B., Strydom, T., Suarez, M.L., Svenning, J.-C., Svitková, I., Svitok, M., Svoboda, M., Swaine, E., Swenson, N., Tabarelli, M., Takagi, K., Tappeiner, U., Tarifa, R., Tauugourdeau, S., Tavsanoglu, C., Beest, M. te, Tedersoo, L., Thiffault, N., Thom, D., Thomas, E., Thompson, K., Thornton, P.E., Thuiller, W., Tichý, L., Tissue, D., Tjoelker, M.G., Tng, D.Y.P., Tobias, J., Török, P., Tarin, T., Torres-Ruiz, J.M., Tóthmérész, B., Treurnicht, M., Trivellone, V., Trolliet, F., Trotsiuk, V., Tsakalos,

J.L., Tsiripidis, I., Tysklind, N., Umehara, T., Usoltsev, V., Vadeboncoeur, M., Vaezi, J., Valladares, F., Vamosi, J., Bodegom, P.M. van, Breugel, M. van, Cleemput, E.V., Weg, M. van de, Merwe, S. van der, Plas, F. van der, Sande, M.T. van der, Kleunen, M. van, Meerbeek, K.V., Vanderwel, M., Vanselow, K.A., Vårhammar, A., Varone, L., Valderrama, M.Y.V., Vassilev, K., Vellend, M., Veneklaas, E.J., Verbeeck, H., Verheyen, K., Vibrans, A., Vieira, I., Villacís, J., Violle, C., Vivek, P., Wagner, K., Waldram, M., Waldron, A., Walker, A.P., Waller, M., Walther, G., Wang, H., Wang, F., Wang, W., Watkins, H., Watkins, J., Weber, U., Weedon, J.T., Wei, L., Weigelt, P., Weiher, E., Wells, A.W., Wellstein, C., Wenk, E., Westoby, M., Westwood, A., White, P.J., Whitten, M., Williams, M., Winkler, D.E., Winter, K., Womack, C., Wright, I.J., Wright, S.J., Wright, J., Pinho, B.X., Ximenes, F., Yamada, T., Yamaji, K., Yanai, R., Yankov, N., Yguel, B., Zanini, K.J., Zanne, A.E., Zelený, D., Zhao, Y.-P., Zheng, Jingming, Zheng, Ji, Ziemińska, K., Zirbel, C.R., Zizka, G., Zo-Bi, I.C., Zotz, G., Wirth, C., 2020. TRY plant trait database – enhanced coverage and open access. Global Change Biology 26, 119–188. https://doi.org/10.1111/gcb.14904

Kennedy, D., Swenson, S., Oleson, K.W., Lawrence, D.M., Fisher, R., Lola da Costa, A.C., Gentine, P., 2019. Implementing Plant Hydraulics in the Community Land Model, Version 5. J. Adv. Model. Earth Syst. 11, 485–513. https://doi.org/10.1029/2018MS001500

Klein, T., 2014. The variability of stomatal sensitivity to leaf water potential across tree species indicates a continuum between isohydric and anisohydric behaviours. Funct Ecol 28, 1313–1320. https://doi.org/10.1111/1365-2435.12289

Li, X., Blackman, C.J., Choat, B., Duursma, R.A., Rymer, P.D., Medlyn, B.E., Tissue, D.T., 2018. Tree hydraulic traits are coordinated and strongly linked to climate-of-origin across a rainfall gradient. Plant, Cell & Environment 41, 646–660. https://doi.org/10.1111/pce.13129

Li, L., Yang, Z.-L., Matheny, A. M., Zheng, H., Swenson, S. C., Lawrence, D. M., et al. (2021). Representation of Plant Hydraulics in the Noah-MP Land Surface Model: Model Development and Multiscale Evaluation. Journal of Advances in Modeling Earth Systems, 13(4), e2020MS002214. https://doi.org/10.1029/2020MS002214

Lin, Y.-S., Medlyn, B.E., Duursma, R.A., Prentice, I.C., Wang, H., Baig, S., Eamus, D., de Dios, V.R., Mitchell, P., Ellsworth, D.S., de Beeck, M.O., Wallin, G., Uddling, J., Tarvainen, L., Linderson, M.-L., Cernusak, L.A., Nippert, J.B., Ocheltree, T.W., Tissue, D.T., Martin-StPaul, N.K., Rogers, A., Warren, J.M., De Angelis, P., Hikosaka, K., Han, Q., Onoda, Y., Gimeno, T.E., Barton, C.V.M., Bennie, J., Bonal, D., Bosc, A., Löw, M., Macinins-Ng, C., Rey, A., Rowland, L., Setterfield, S.A., Tausz-Posch, S., Zaragoza-Castells, J., Broadmeadow, M.S.J., Drake, J.E., Freeman, M., Ghannoum, O., Hutley, L.B., Kelly, J.W., Kikuzawa, K., Kolari, P., Koyama, K., Limousin, J.-M., Meir, P., Lola da Costa, A.C., Mikkelsen, T.N., Salinas, N., Sun, W., Wingate, L., 2015. Optimal stomatal behaviour around the world. Nature Climate Change 5, 459–464. https://doi.org/10.1038/nclimate2550

Liu, Y., Holtzman, N. M., & Konings, A. G. (2021). Global ecosystem-scale plant hydraulic traits retrieved using model–data fusion. Hydrology and Earth System Sciences, 25(5), 2399–2417. https://doi.org/10.5194/hess-25-2399-2021

948 Liu, Y., Kumar, M., Katul, G.G., Feng, X., Konings, A.G., 2020. Plant hydraulics accentuates
949 the effect of atmospheric moisture stress on transpiration. Nature Climate Change 10,
950 691–695. https://doi.org/10.1038/s41558-020-0781-5
951 Luo, Y., Ogle, K., Tucker, C., Fei, S., Gao, C., LaDeau, S., Clark, J.S., Schimel, D.S., 2011.
952 Ecological forecasting and data assimilation in a data-rich era. Ecological Applications
953 21, 1429–1442. https://doi.org/10.1890/09-1275.1
954 Luo, Y., Weng, E., Wu, X., Gao, C., Zhou, X., Zhang, L., 2009. Parameter Identifiability,
955 Constraint, and Equifinality in Data Assimilation with Ecosystem Models. Ecological
956 Applications 19, 571–574.
957 Maherali, H., Moura, C. E., Caldeira, M. C., Willson, C. J., & Jackson, R. B. (2006). Functional
958 coordination between leaf gas exchange and vulnerability to xylem cavitation in
959 temperate forest trees. Plant, Cell & Environment, 29(4), 571–583.
960 https://doi.org/10.1111/j.1365-3040.2005.01433.x
961 Manzoni, S., Vico, G., Katul, G., Fay, P. A., Polley, W., Palmroth, S., Porporato, A., 2011.
962 Optimizing stomatal conductance for maximum carbon gain under water stress: a meta-
963 analysis across plant functional types and climates. Functional Ecology, 25(3), 456–467.
964 https://doi.org/10.1111/j.1365-2435.2010.01822.x
965 Martínez-Vilalta, J., Cochard, H., Mencuccini, M., Sterck, F., Herrero, A., Korhonen, J.F.J.,
966 Llorens, P., Nikinmaa, E., Nolè, A., Poyatos, R., Ripullone, F., Sass-Klaassen, U.,
967 Zweifel, R., 2009. Hydraulic adjustment of Scots pine across Europe. New Phytologist
968 184, 353–364. https://doi.org/10.1111/j.1469-8137.2009.02954.x
969 Martin-StPaul, N., Delzon, S., Cochard, H., 2017. Plant resistance to drought depends on timely
970 stomatal closure. Ecology Letters 20, 1437–1447. https://doi.org/10.1111/ele.12851

971 Matheny, A.M., Bohrer, G., Vogel, C.S., Morin, T.H., He, L., Frasson, R.P. de M.,
972 Mirfenderesgi, G., Schäfer, K.V.R., Gough, C.M., Ivanov, V.Y., Curtis, P.S., 2014.
973 Species-specific transpiration responses to intermediate disturbance in a northern
974 hardwood forest. Journal of Geophysical Research: Biogeosciences 119, 2292–2311.
975 https://doi.org/10.1002/2014JG002804
976 Matheny, A.M., Fiorella, R.P., Bohrer, G., Poulsen, C.J., Morin, T.H., Wunderlich, A., Vogel,
977 C.S., Curtis, P.S., 2017. Contrasting strategies of hydraulic control in two codominant
978 temperate tree species. Ecohydrology 10, e1815. https://doi.org/10.1002/eco.1815
979 McDowell, N.G., Allen, C.D., 2015. Darcy's law predicts widespread forest mortality under
980 climate warming. Nature Climate Change 5, 669–672.
981 https://doi.org/10.1038/nclimate2641
982 McLaughlin, B.C., Blakey, R., Weitz, A.P., Feng, X., Brown, B.J., Ackerly, D.D., Dawson, T.E.,
983 Thompson, S.E., 2020. Weather underground: Subsurface hydrologic processes mediate
984 tree vulnerability to extreme climatic drought. Global Change Biology 26, 3091–3107.
985 https://doi.org/10.1111/gcb.15026
986 Medlyn, B.E., Duursma, R.A., Eamus, D., Ellsworth, D.S., Prentice, I.C., Barton, C.V.M., Crous,
987 K.Y., De Angelis, P., Freeman, M., Wingate, L., 2011. Reconciling the optimal and
988 empirical approaches to modelling stomatal conductance. Global Change Biology 17,
989 2134–2144. https://doi.org/10.1111/j.1365-2486.2010.02375.x
990 Mencuccini, M., Manzoni, S., Christoffersen, B., 2019. Modelling water fluxes in plants: from
991 tissues to biosphere. New Phytologist. https://doi.org/10.1111/nph.15681
992 Mirfenderesgi, G., Matheny, A.M., Bohrer, G., 2019. Hydrodynamic trait coordination and cost-
993 benefit trade-offs throughout the isohydric-anisohydric continuum in trees:

994 Hydrodynamic Trait Coordination and Cost-Benefit Trade-offs in Trees. Ecohydrology
995 12, e2041. https://doi.org/10.1002/eco.2041
996 Mo, X., Chen, J.M., Ju, W., Black, T.A., 2008. Optimization of ecosystem model parameters
997 through assimilating eddy covariance flux data with an ensemble Kalman filter.
998 Ecological Modelling 217, 157–173. https://doi.org/10.1016/j.ecolmodel.2008.06.021
999 Monteith, J.L., Unsworth, M.H. (Eds.), 2013. Principles of Environmental Physics, in: Principles
1000 of Environmental Physics (Fourth Edition). Academic Press, Boston, p. i.
1001 https://doi.org/10.1016/B978-0-12-386910-4.00018-4
1002 Nave, L.E., Gough, C.M., Maurer, K.D., Bohrer, G., Hardiman, B.S., Moine, J.L., Munoz, A.B.,
1003 Nadelhoffer, K.J., Sparks, J.P., Strahm, B.D., Vogel, C.S., Curtis, P.S., 2011. Disturbance
1004 and the resilience of coupled carbon and nitrogen cycling in a north temperate forest.
1005 Journal of Geophysical Research: Biogeosciences 116.
1006 https://doi.org/10.1029/2011JG001758
1007 Novick, K.A., Ficklin, D.L., Stoy, P.C., Williams, C.A., Bohrer, G., Oishi, A.C., Papuga, S.A.,
1008 Blanken, P.D., Noormets, A., Sulman, B.N., Scott, R.L., Wang, L., Phillips, R.P., 2016.
1009 The increasing importance of atmospheric demand for ecosystem water and carbon
1010 fluxes. Nature Climate Change 6, 1023–1027. https://doi.org/10.1038/nclimate3114
1011 Novick, K.A., Konings, A.G., Gentine, P., 2019. Beyond soil water potential: An expanded view
1012 on isohydricity including land–atmosphere interactions and phenology. Plant, Cell &
1013 Environment 42, 1802–1815. https://doi.org/10.1111/pce.13517
1014 Paschalis, A., Fatichi, S., Zscheischler, J., Ciais, P., Bahn, M., Boysen, L., Chang, J., Kauwe,
1015 M.D., Estiarte, M., Goll, D., Hanson, P.J., Harper, A.B., Hou, E., Kigel, J., Knapp, A.K.,
1016 Larsen, K.S., Li, W., Lienert, S., Luo, Y., Meir, P., Nabel, J.E.M.S., Ogaya, R., Parolari,

A.J., Peng, C., Peñuelas, J., Pongratz, J., Rambal, S., Schmidt, I.K., Shi, H., Sternberg, M., Tian, H., Tschumi, E., Ukkola, A., Vicca, S., Viovy, N., Wang, Y.-P., Wang, Z., Williams, K., Wu, D., Zhu, Q., 2020. Rainfall manipulation experiments as simulated by terrestrial biosphere models: Where do we stand? Global Change Biology 26, 3336–3355. https://doi.org/10.1111/gcb.15024

Patil, A., Huard, D., Fonnesbeck, C., 2010. PyMC: Bayesian Stochastic Modelling in Python. J. Stat. Soft. 35. https://doi.org/10.18637/jss.v035.i04

Powell, T.L., Galbraith, D.R., Christoffersen, B.O., Harper, A., Imbuzeiro, H.M.A., Rowland, L., Almeida, S., Brando, P.M., Costa, A.C.L. da, Costa, M.H., Levine, N.M., Malhi, Y., Saleska, S.R., Sotta, E., Williams, M., Meir, P., Moorcroft, P.R., 2013. Confronting model predictions of carbon fluxes with measurements of Amazon forests subjected to experimental drought. New Phytologist 200, 350–365. https://doi.org/10.1111/nph.12390

Poyatos, R., Granda, V., Flo, V., Adams, M.A., Adorján, B., Aguadé, D., Aidar, M.P.M., Allen, S., Alvarado-Barrientos, M.S., Anderson-Teixeira, K.J., Aparecido, L.M., Arain, M.A., Aranda, I., Asbjornsen, H., Baxter, R., Beamesderfer, E., Berry, Z.C., Berveiller, D., Blakely, B., Boggs, J., Bohrer, G., Bolstad, P.V., Bonal, D., Bracho, R., Brito, P., Brodeur, J., Casanoves, F., Chave, J., Chen, H., Cisneros, C., Clark, K., Cremonese, E., David, J.S., David, T.S., Delpierre, N., Desai, A.R., Do, F.C., Dohnal, M., Domec, J.-C., Dzikiti, S., Edgar, C., Eichstaedt, R., El-Madany, T.S., Elbers, J., Eller, C.B., Euskirchen, E.S., Ewers, B., Fonti, P., Forner, A., Forrester, D.I., Freitas, H.C., Galvagno, M., Garcia-Tejera, O., Ghimire, C.P., Gimeno, T.E., Grace, J., Granier, A., Griebel, A., Guangyu, Y., Gush, M.B., Hanson, P., Hasselquist, N.J., Heinrich, I., Hernandez-Santana, V., Herrmann, V., Hölttä, T., Holwerda, F., Hongzhong, D., Irvine, J., Isarangkool Na

Ayutthaya, S., Jarvis, P.G., Jochheim, H., Joly, C.A., Kaplick, J., Kim, H.S., Klemedtsson, L., Kropp, H., Lagergren, F., Lane, P., Lang, P., Lapenas, A., Lechuga, V., Lee, M., Leuschner, C., Limousin, J.-M., Linares, J.C., Linderson, M.-L., Lindroth, A., Llorens, P., López-Bernal, Á., Loranty, M.M., Lüttschwager, D., Macinnis-Ng, C., Maréchaux, I., Martin, T.A., Matheny, A., McDowell, N., McMahon, S., Meir, P., Mészáros, I., Migliavacca, M., Mitchell, P., Mölder, M., Montagnani, L., Moore, G.W., Nakada, R., Niu, F., Nolan, R.H., Norby, R., Novick, K., Oberhuber, W., Obojes, N., Oishi, C.A., Oliveira, R.S., Oren, R., Ourcival, J.-M., Paljakka, T., Perez-Priego, O., Peri, P.L., Peters, R.L., Pfautsch, S., Pockman, W.T., Preisler, Y., Rascher, K., Robinson, G., Rocha, H., Rocheteau, A., Röll, A., Rosado, B., Rowland, L., Rubtsov, A.V., Sabaté, S., Salmon, Y., Salomón, R.L., Sánchez-Costa, E., Schäfer, K.V.R., Schuldt, B., Shashkin, A., Stahl, C., Stojanović, M., Suárez, J.C., Sun, G., Szatniewska, J., Tatarinov, F., Tesař, M., Thomas, F.M., Tor-ngern, P., Urban, J., Valladares, F., van der Tol, C., van Meerveld, I., Varlagin, A., Voigt, H., Warren, J., Werner, C., Werner, W., Wieser, G., Wingate, L., Wullschleger, S., Yi, K., Zweifel, R., Steppe, K., Mencuccini, M., Martínez-Vilalta, J., 2020. Global transpiration data from sap flow measurements: the SAPFLUXNET database. Earth System Science Data Discussions 1–57. https://doi.org/10.5194/essd-2020-227

Poyatos, R., Granda, V., Molowny-Horas, R., Mencuccini, M., Steppe, K., Martínez-Vilalta, J., 2016. SAPFLUXNET: towards a global database of sap flow measurements. Tree Physiology 36, 1449–1455. https://doi.org/10.1093/treephys/tpw110

Pritzkow, C., Williamson, V., Szota, C., Trouvé, R., Arndt, S.K., 2020. Phenotypic plasticity and genetic adaptation of functional traits influences intra-specific variation in hydraulic efficiency and safety. Tree Physiol 40, 215–229. https://doi.org/10.1093/treephys/tpz121

Rafael Poyatos, Víctor Granda, Víctor Flo, Roberto Molowny-Horas, Kathy Steppe, Maurizio Mencuccini, Jordi Martínez-Vilalta, 2019. SAPFLUXNET: A global database of sap flow measurements. https://doi.org/10.5281/zenodo.2530798

Raupach, M.R., Rayner, P.J., Barrett, D.J., DeFries, R.S., Heimann, M., Ojima, D.S., Quegan, S., Schmullius, C.C., 2005. Model–data synthesis in terrestrial carbon observation: methods, data requirements and data uncertainty specifications. Global Change Biology 11, 378–397. https://doi.org/10.1111/j.1365-2486.2005.00917.x

Rosas, T., Mencuccini, M., Barba, J., Cochard, H., Saura-Mas, S., Martínez-Vilalta, J., 2019. Adjustments and coordination of hydraulic, leaf and stem traits along a water availability gradient. New Phytologist 223, 632–646. https://doi.org/10.1111/nph.15684

Sabot, M.E.B., Kauwe, M.G.D., Pitman, A.J., Medlyn, B.E., Verhoef, A., Ukkola, A.M., Abramowitz, G., 2020. Plant profit maximization improves predictions of European forest responses to drought. New Phytologist 226, 1638–1655. https://doi.org/10.1111/nph.16376

Seabold, S., & Perktold, J. (2010). statsmodels: Econometric and statistical modeling with python. In 9th Python in Science Conference.

Sloan, B. P., Thompson, S. E., & Feng, X. (2021). Plant hydraulic transport controls transpiration sensitivity to soil water stress. Hydrology and Earth System Sciences, 25(8), 4259–4274. https://doi.org/10.5194/hess-25-4259-2021

Sobol, I.M., 2001. Global sensitivity indices for nonlinear mathematical models and their Monte Carlo estimates. Mathematics and Computers in Simulation, The Second IMACS Seminar on Monte Carlo Methods 55, 271–280. https://doi.org/10.1016/S0378-4754(00)00270-6

Sperry, J.S., Adler, F.R., Campbell, G.S., Comstock, J.P., 1998. Limitation of plant water use by rhizosphere and xylem conductance: results from a model. Plant, Cell & Environment 21, 347–359. https://doi.org/10.1046/j.1365-3040.1998.00287.x

Thomsen, J.E., Bohrer, G., Matheny, A.M., Ivanov, V.Y., He, L., Renninger, H.J., Schäfer, K.V.R., 2013. Contrasting Hydraulic Strategies during Dry Soil Conditions in Quercus rubra and Acer rubrum in a Sandy Site in Michigan. Forests 4, 1106–1120. https://doi.org/10.3390/f4041106

Trugman, A.T., Anderegg, L.D.L., Wolfe, B.T., Birami, B., Ruehr, N.K., Detto, M., Bartlett, M.K., Anderegg, W.R.L., 2019. Climate and plant trait strategies determine tree carbon allocation to leaves and mediate future forest productivity. Global Change Biology 25, 3395–3405. https://doi.org/10.1111/gcb.14680

Trugman, A.T., Medvigy, D., Mankin, J.S., Anderegg, W.R.L., 2018. Soil Moisture Stress as a Major Driver of Carbon Cycle Uncertainty. Geophysical Research Letters 45, 6495–6503. https://doi.org/10.1029/2018GL078131

Tyree, M.T., Sperry, J.S., 1988. Do Woody Plants Operate Near the Point of Catastrophic Xylem Dysfunction Caused by Dynamic Water Stress? Answers from a Model. Plant Physiol. 88, 574–580. https://doi.org/10.1104/pp.88.3.574

van Genuchten, M.Th., 1980. CLOSED-FORM EQUATION FOR PREDICTING THE HYDRAULIC CONDUCTIVITY OF UNSATURATED SOILS. Soil Science Society of America Journal 44, 892–898.

Williams, P.A., Allen, C.D., Macalady, A.K., Griffin, D., Woodhouse, C.A., Meko, D.M., Swetnam, T.W., Rauscher, S.A., Seager, R., Grissino-Mayer, H.D., Dean, J.S., Cook, E.R., Gangodagamage, C., Cai, M., McDowell, N.G., 2013. Temperature as a potent driver of regional forest drought stress and tree mortality. Nature Climate Change 3, 292–297. https://doi.org/10.1038/nclimate1693

Wolf, A., Anderegg, W. R. L., Pacala, S. W., 2016. Optimal stomatal behavior with competition for water and risk of hydraulic impairment. Proceedings of the National Academy of Sciences of the United States of America, 113(46), E7222–E7230. https://doi.org/10.1073/pnas.1615144113

Wu, Y., Liu, S., Huang, Z., Yan, W., 2014. Parameter optimization, sensitivity, and uncertainty analysis of an ecosystem model at a forest flux tower site in the United States. J. Adv. Model. Earth Syst. 6, 405–419. https://doi.org/10.1002/2013MS000298

Xiao, J., Davis, K.J., Urban, N.M., Keller, K., 2014. Uncertainty in model parameters and regional carbon fluxes: A model-data fusion approach. Agricultural and Forest Meteorology 189–190, 175–186. https://doi.org/10.1016/j.agrformet.2014.01.022

Xu, X., Medvigy, D., Powers, J. S., Becknell, J. M., & Guan, K., 2016. Diversity in plant hydraulic traits explains seasonal and inter-annual variations of vegetation dynamics in seasonally dry tropical forests. New Phytologist, 212(1), 80–95. https://doi.org/10.1111/nph.14009

Young, D.J.N., Stevens, J.T., Earles, J.M., Moore, J., Ellis, A., Jirka, A.L., Latimer, A.M., 2017. Long-term climate and competition explain forest mortality patterns under extreme drought. Ecol Lett 20, 78–86. https://doi.org/10.1111/ele.12711

Zhou, S., Duursma, R. A., Medlyn, B. E., Kelly, J. W. G., Prentice, I. C., 2013. How should we model plant responses to drought? An analysis of stomatal and non-stomatal responses to water stress. Agricultural and Forest Meteorology, 182–183, 204–214. https://doi.org/10.1016/J.AGRFORMET.2013.05.009

Zhu, Q., Castellano, M.J., Yang, G., 2018. Coupling soil water processes and the nitrogen cycle across spatial scales: Potentials, bottlenecks and solutions. Earth-Science Reviews 187, 248–258. https://doi.org/10.1016/j.earscirev.2018.10.005

Supporting information

Multi-segment xylem model

Let us compare a whole-plant model with a single segment from a multi-segment model. Assuming they have the same flux, we get

$$k_{whole}(\Psi_{whole}, \Psi_{50whole})\Delta\Psi_{whole} = k_{segment}\left(\Psi_{segment}, \Psi_{50segment}\right)\Delta\Psi_{segment}$$

where k, Ψ, and $\Delta\Psi$ denote the plant hydraulic conductance, plant water potential, and the water potential gradient, respectively; and the subscripts, whole and segment, represent the two corresponding models.

As it is fair to consider

$$\Delta\Psi_{whole} > \Delta\Psi_{segment},$$

it follows

$$k_{whole}(\Psi_{whole}, \Psi_{50whole}) < k_{segment}\left(\Psi_{segment}, \Psi_{50segment}\right).$$

The above inequality suggests that the whole plant model has a more vulnerable xylem (*i.e.,* $\Psi_{50whole} > \Psi_{50segment}$) and/or a more negative water potential (*i.e.,* $\Psi_{whole} < \Psi_{segment}$). Alternatively, the above inequality can also be satisfied with the whole plant model having a stronger xylem (*i.e.,* $\Psi_{50whole} < \Psi_{50segment}$), which is more likely when Ψ_{whole} is much lower than $\Psi_{segment}$. This later scenario is more realistic when comparing the whole plant model with the segment that is close to the root (as the water potential there is close to the soil water potential) in a multi-segment model.

We explored the above ideas with a simple simulation experiment. In this experiment, we assume that 1) the two models share the soil water potential and 2) the water potential drop in the whole-plant model is larger than that in the multi-segment model.

As shown in Fig. S1, given the P50 for the whole plant model (red) and water potential drops for the two models, we found that the inferred P50 for each segment in the multi-segment model becomes more negative for the segments that are further away from the soil where the red horizontal dashed line indicates the given value for the P50 for the whole plant model and the first segment is the segment that contains the fine roots.

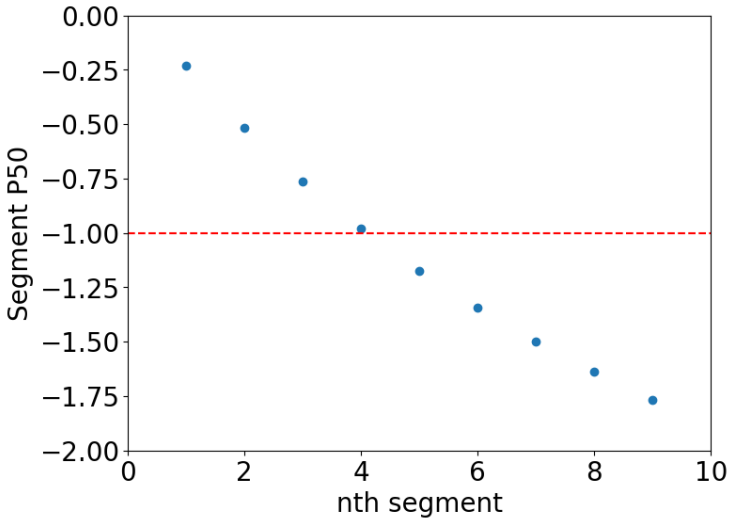

Figure S1. P50 at each segment in a plant with n (=10) segments. The horizontal red dashed line indicates the corresponding whole-plant P50 value.

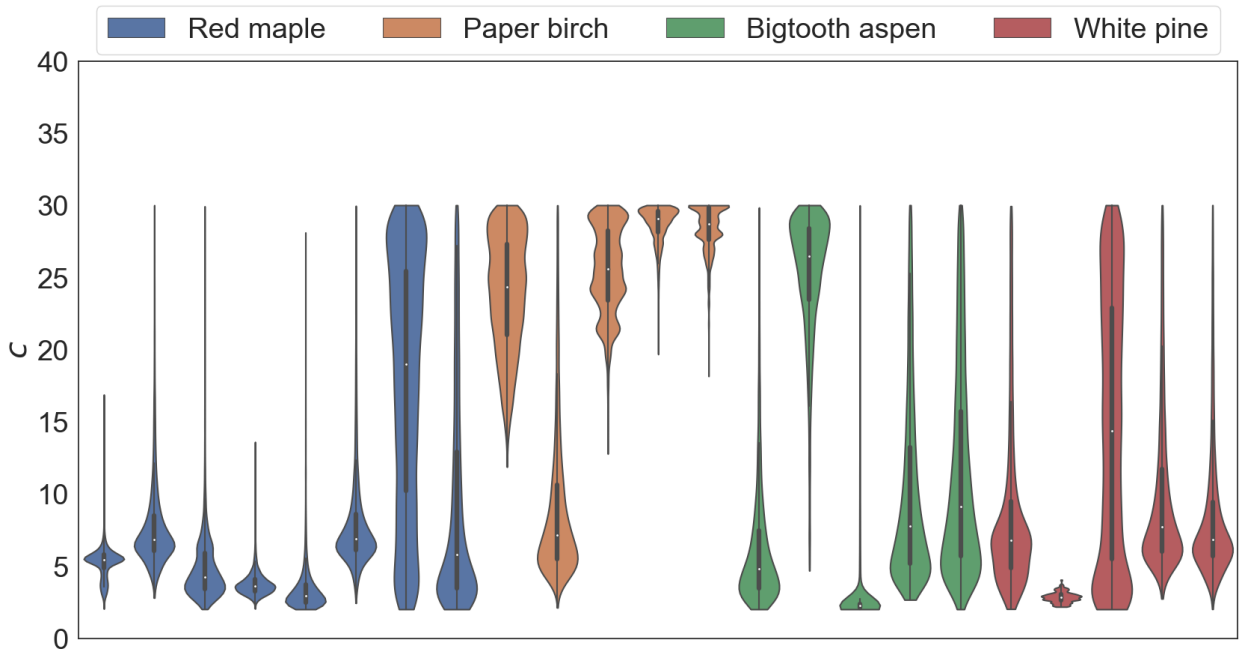

Figure S2. Posterior distributions of *c* with prior distribution as Uniform [2, 30]. Each bar represents an individual tree. Color indicates species: blue for red maple, yellow for paper birch, green for bigtooth aspen, and red for white pine.

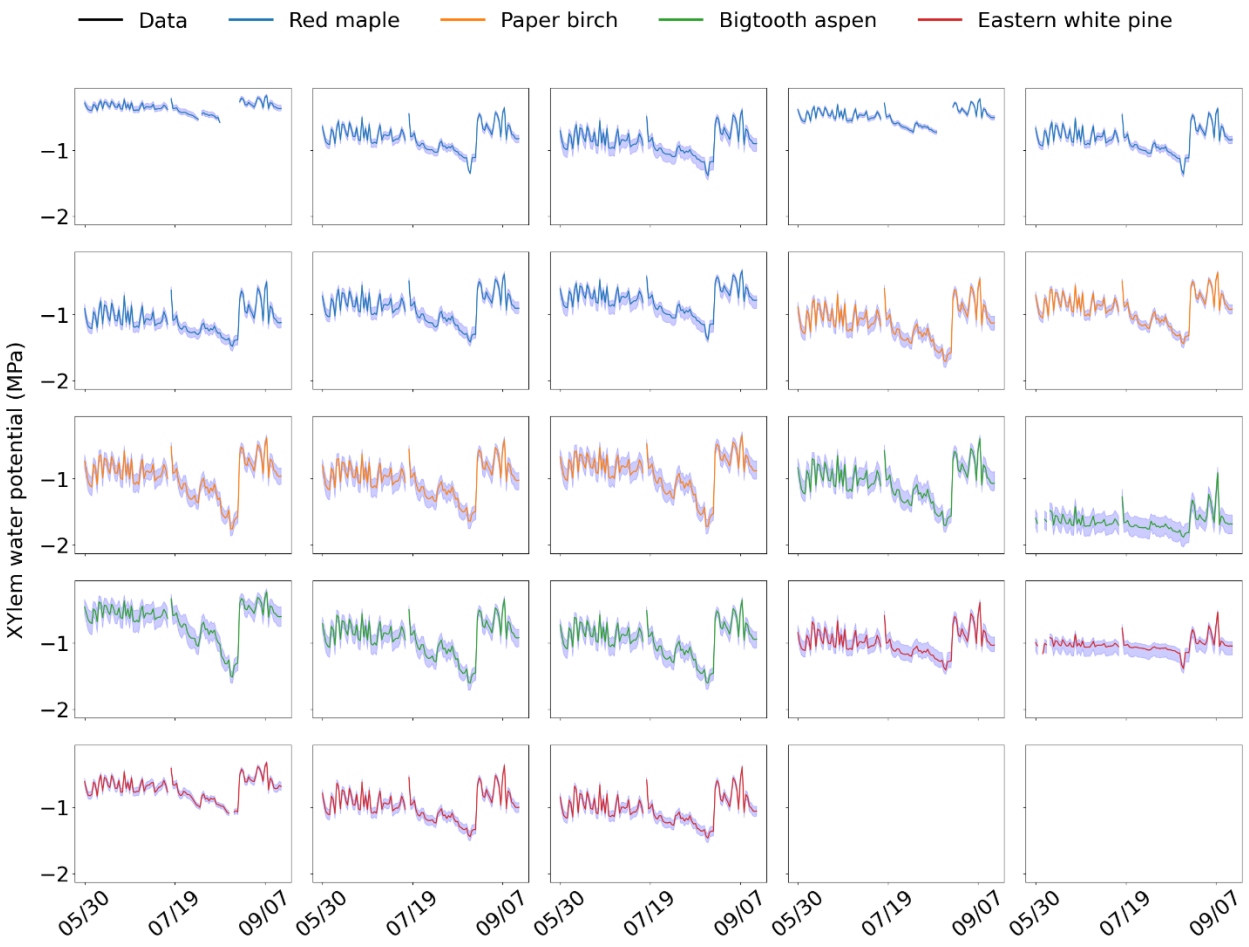

1171

1172 **Figure S3**. Estimates of plant water potential over time. The 5th, 50th, and 95th percentiles of

1173 1000 MCMC estimates of plant water potential are shown. Color indicates species (blue: red

1174 maple; brown: paper birch; green: bigtooth aspen; red: white pine). Similar ranges in xylem

1175 water potentials (0 to -0.6MPa) are observed for red maple species in a different year (Thomsen

1176 2013) for a number of our red maple individuals.

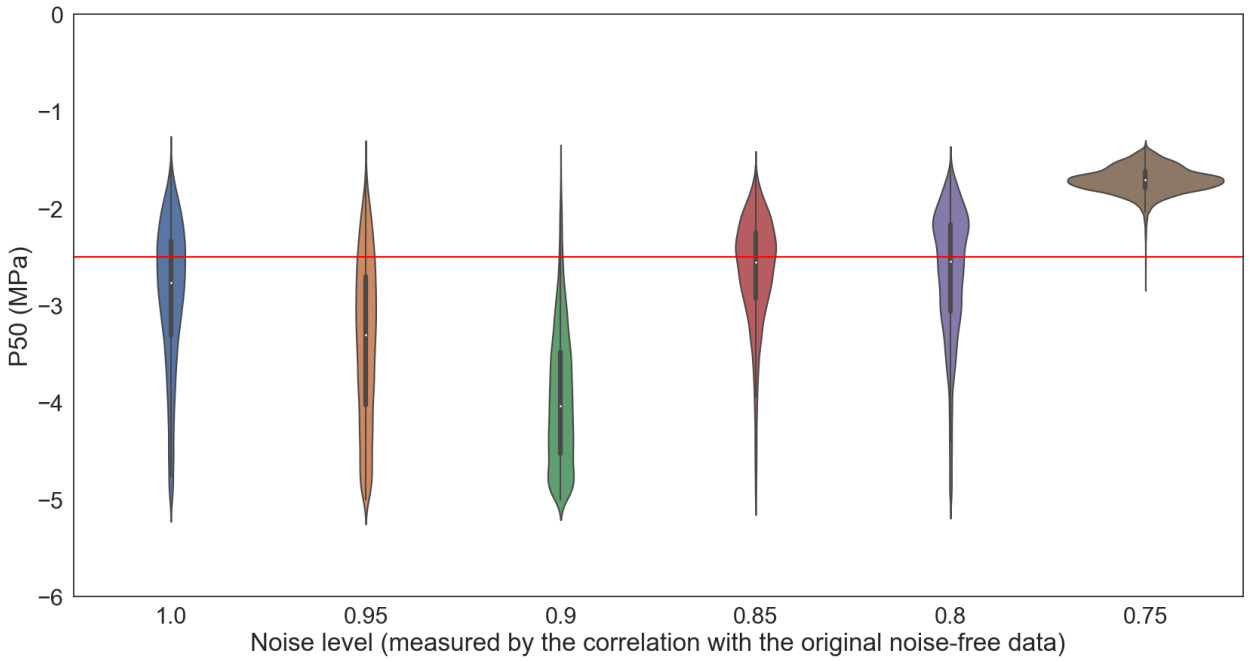

Figure S4. Posterior distributions of P50 inferred using sap flow data at different noise levels. The horizontal line labels the synthetic truth.

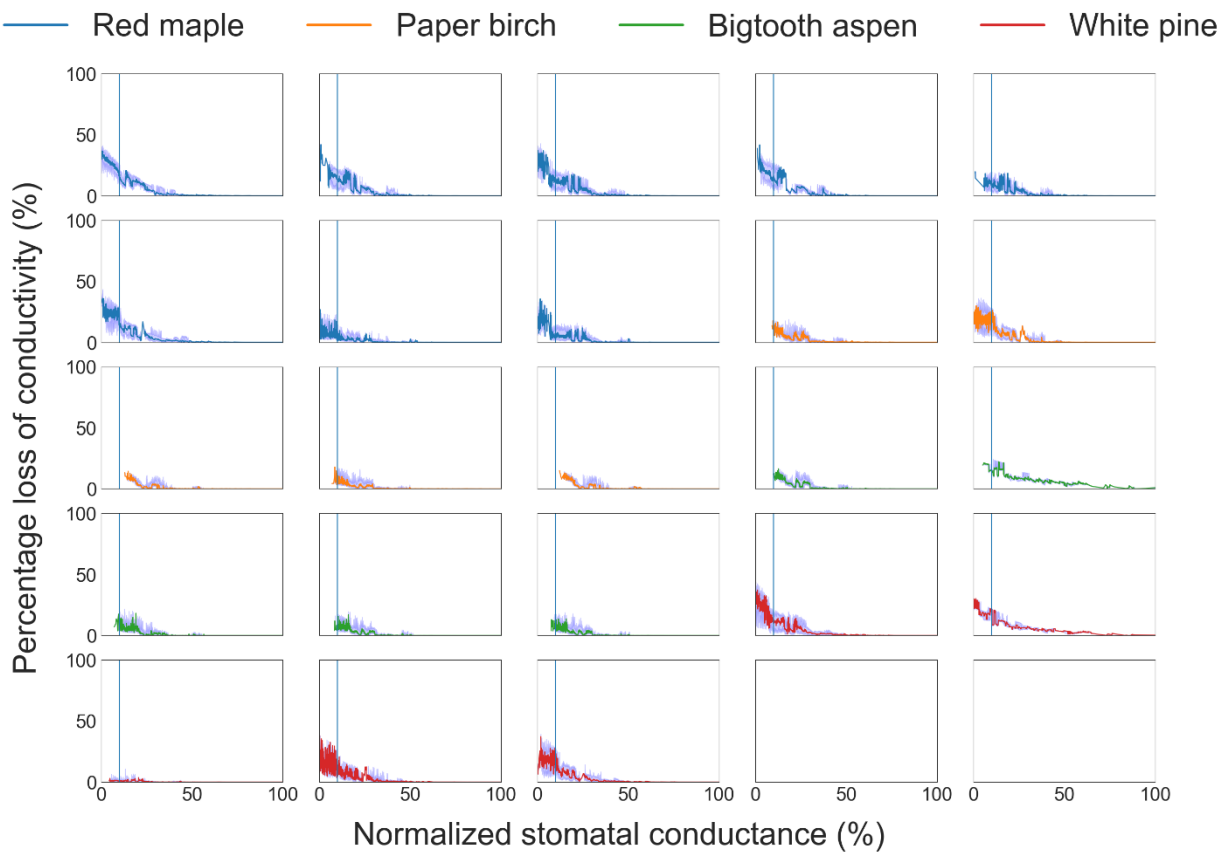

1180

1181 **Figure S5**. Estimates of PLC given stomatal closure. The 5th, 50th, and 95th percentiles of 1000

1182 MCMC estimates of PLC are shown. Color indicates species (blue: red maple; brown: paper

1183 birch; green: bigtooth aspen; red: white pine). The vertical line indicates 90% stomatal closure.

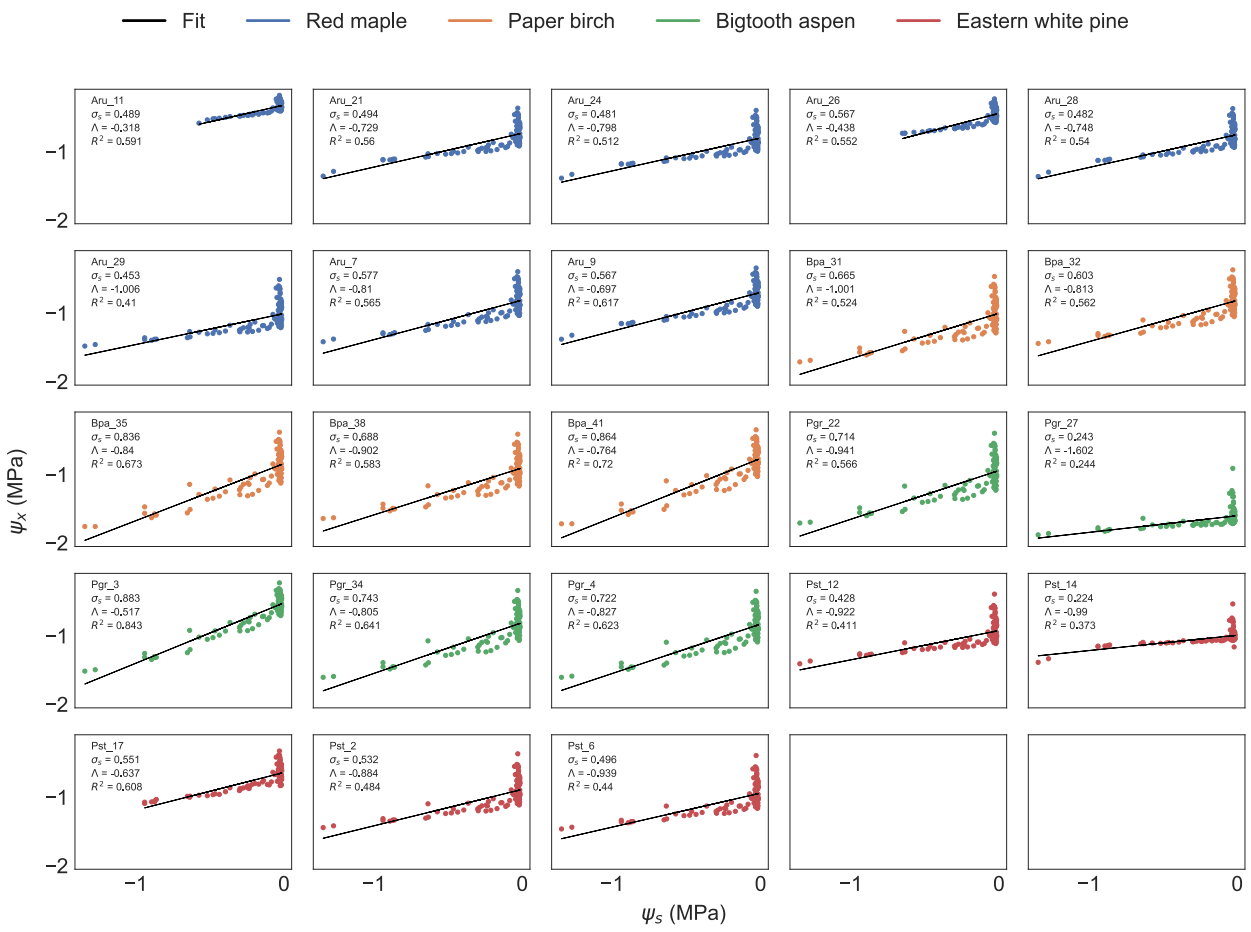

Figure S6. Linear relation between inferred plant water potential to observed soil water potential used to identify the isohydricity index σ (slope) for each site (see Sect. 2.6 for details). Color indicates species (blue: red maple; brown: paper birch; green: bigtooth aspen; red: white pine). The site ID, slope (σ), intercept (Λ), and coefficient of determination (R^2) are shown for each site. The σ values are used to create Figure 6a in the main text.

Multiple Comparison of Means - Tukey HSD, FWER=0.05

group1	group2	meandiff	p-adj	lower	upper	reject
Bigtooth aspen	Eastern white pine	-0.2147	0.1081	-0.4647	0.0353	False
Bigtooth aspen	Paper birch	0.0704	0.8448	-0.1796	0.3203	False
Bigtooth aspen	Red maple	-0.1472	0.2878	-0.3725	0.0782	False
Eastern white pine	Paper birch	0.2851	0.0221	0.0351	0.5351	True
Eastern white pine	Red maple	0.0675	0.8169	-0.1578	0.2929	False
Paper birch	Red maple	-0.2175	0.0608	-0.4429	0.0078	False

Figure S7. Output for pairwise t-tests performed in Tukey's HSD test by the Python package *statsmodel*.